SYNTHESIS AND CHARACTERIZATION OF PIEZO-MAGNETO (PVDF - FE_3O_4) COMPOSITES

A Thesis

by

OLIVER KASONGO MULAMBA

Submitted to the Office of Graduate Studies of
Texas A&M University
in partial fulfillment of the requirements for the degree of

MASTER OF SCIENCE

May 2011

Major Subject: Mechanical Engineering

SYNTHESIS AND CHARACTERIZATION OF PIEZO-MAGNETO (PVDF - FE_3O_4) COMPOSITES

A Thesis

by

OLIVER KASONGO MULAMBA

Submitted to the Office of Graduate Studies of
Texas A&M University
in partial fulfillment of the requirements for the degree of

MASTER OF SCIENCE

Approved by:

Chair of Committee,	Hong Liang
Committee Members,	Julie Linsey
	Miladin Radovic
Head of Department,	Dennis O'Neal

May 2011

Major Subject: Mechanical Engineering

ABSTRACT

Synthesis and Characterization of Piezo-Magneto (PVDF - Fe_3O_4) Composites.

(May 2011)

Oliver Kasongo Mulamba, B.S., West Texas A&M

Chair of Advisory Committee: Dr. Hong Liang

This research entails the synthesis and characterization of a novel class of materials which incorporate both magnetic and piezoelectric characteristics. The composite is made up of the piezoelectric polymer PVDF and magnetic nanoparticles.

The testing samples are produced using a spin casting process. The characterizations of the samples were performed using X-ray diffraction, Atomic force microscopy, linear staging, Dynamic mechanical analysis, Differential scanning calorimetry, and Fourier transform Infra-Red. X-ray diffraction and Atomic force microscopy showed that the presence of the Fe_3O_4 particles have no effect on the crystallinity of the polymer matrix, therefore allowing for the incorporation of inclusions without directly affecting the piezoelectric property. Changes in the thermal characteristics of the polymer matrix, observed using Differential scanning calorimetry, indicated increases in the thermal conductivity of the composite. Decreases in the heat of melting and crystallization were also observed and further solidified the conclusion that the presence of the Fe_3O_4 nanoparticles changes the thermal behavior of the polymer. It was observed from the DMA results that the presence of the Fe_3O_4 nanoparticles caused

an increase in the storage modulus of the polymer matrix which is related to an increase in the material's ability to store energy. Linear staging results showed that presence of the nanoparticles had an effect on the mechanical properties of the composites and altered the time dependent voltage output readings. These results were used to calculate the energy capabilities of the composite material and it was found that the composites showed greater energy outputs with increasing amounts of nanoparticles. Interaction was observed between the embedded particles and an external magnetic field, which was found to decrease the energy outputs of the composites.

This research showed enhancements in the composite material's energy outputs in comparison to the pure PVDF samples. This research also showed that the embedded nanoparticles interacted with an exteriorly applied magnetic field. This observation introduces a new dimension of possible activation processes for piezoelectric devices which have been largely based on physical forms of activation. PVDF which is widely used in research and applications for its superior output capabilities has been enhanced in this research and shown to have capabilities to exhibit higher energy outputs.

DEDICATION

I dedicate this thesis to my brother, Chappy Charles Mulamba; your influence on my life is beyond what words could express. To my parents, Raphael and Benita; your unfaltering faith and belief in me has molded me into a man I never thought I could be. To Greg ‘Prince Goyo’ , Teddy ‘Ted Breezy’, Peter ‘My Quarterback’, Patrick ‘The Tyzon’ and Floride ‘Kalala Flo Jo’. We are COB forget the EOPs, Jeremiah 29:11.

ACKNOWLEDGEMENTS

I would like to acknowledge my Lord and savior Jesus Christ for I know that without his blessing and guidance, this thesis would not be a reality. May my work bring glory and honor to him whose will is my purpose.

I would like to thank my committee chair, Dr. Liang, for her guidance and support throughout the course of this research.

A special thanks to Dr. Emily Hunt, I could never express my gratitude enough. Your example, your belief in me and your advice have been a cornerstone in my growth.

Thanks also go to my friends and colleagues and the department faculty and staff for making my time at Texas A&M University a great experience. I also want to extend my gratitude to the Pathways fellowship that made the acquisition of my degree a possibility through their generous assistance.

Finally, thanks to my mother and father for their encouragement, love and continued support.

NOMENCLATURE

AFM	Atomic force microscope
c	Velocity of light
d	Distance between parallel lattice planes
D	Volumetric charge density
d_{ij}	Piezoelectric strain constant
DMA	Dynamic mechanical analysis
DMSO	Dimethylsulphoxide
DSC	Differential scanning calorimetry
E	Electric field
e	Stress constant
g_{ij}	Piezoelectric voltage constant
h	Strain constant
k	Force constant,
n	Order of a reflection
PVDF	Poly(vinylidene fluoride)
s	Material compliance
S	Strain
T G+T G− 3 3	γ and ε phases
TG+TG−	α and δ phases
TGA	Thermal gravimetric analysis

TTT	β phase
X	Stress
XRD	X-ray diffraction
ε	Permittivity
θ	Angle between the incident beam and a lattice plane
κ	Permittivity tensor
λ	Wavelength of X-ray
μ	$1\ m\ 2\ m\ /(\ 1\ m + 2\ m\ )$

TABLE OF CONTENTS

Page

Page

LIST OF FIGURES

Page

Page

Page

LIST OF TABLES

Page

CHAPTER I

INTRODUCTION

This chapter introduces the background necessary to understand the purpose and direction of this research. The growth of micro-applications, their use and need for smaller sources of energy is observed. The need for more refined ways of energy harvesting and storage is presented. Another demand is to seek out and develop materials with multi-functionality. The materials and applications that are currently in use, in applications or research, are discussed. This chapter will discuss the properties of the piezoelectric polymer, PVDF, and the magnetic Fe_3O_4 nanoparticles. The discussion will lean to the potential of developing a novel multi-functional composite using these two materials.

1.1. Introduction to Energy Use in Micro-applications

The electronic industry was revolutionized in the mid 20^{th} century, through the development of Integrated Circuits (ICs). These ICs proved to be cost efficient and to have low power consumption in comparison to its high output performance. This was attributed to the small sizes of these components and their ability to quickly switch. The booming years of these components were between 1946-2007, during which their performance was increased and the physical sizes greatly decreased. ICs were the platform upon which Micro-Electro-Mechanical Systems (MEMS) were built. This

---

This thesis follows the style of *IEEE Journal of Oceanic Engineering*.

technology is primarily focused on extremely small mechanical devices that are powered by a source of electricity. This technology is used in a variety of applications:

- Inkjet printers
- Airbag systems in vehicles
- Electronic gaming devices
- Cell phones and IPods
- Bio-MEMS medical technologies

The impact of these devices can be seen in the yearly growth of their financial turnovers as shown in Figure 1. With 14% annual growth and a worth of around $6 billion in 2006, the anticipated growth is phenomenal [1]. One interesting thing to notice is that the majority of developing technologies are shrinking in size. The μ-Fuel cells have attracted a lot of attention in terms of its possibilities, but what must not be overlooked is with the shrinking of the technologies there comes a need for energy sources of reduced dimensions as well.

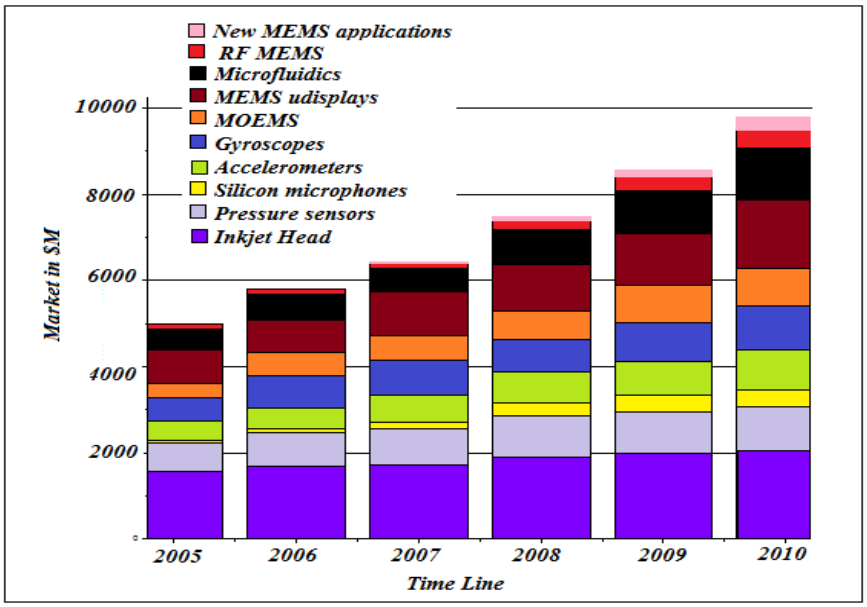

Figure 1: MEMS evolution (adapted from Yole development study)[1]

Renewable energy provides a very possible solution to providing an energy source required by these applications. Renewable energy refers to generating electrical energy from many naturally available sources like the sun, the wind and so on. This capability has caused a massive increase in the manner by which to acquire and utilize these different energies.The north west areas of Texas are well known from extremely windy conditions and so presently the majority of open areas are layered with wind farms to make use of this energy. Areas with higher constant temperatures like the more desert like areas have observed increases in solar panel uses for energy harvesting. The increased use of renewable energy is plausible, even though it's a fairly new technology studies showed that in 2006 18% of global power consumption came from the renewable energy sector[1]. Renewable energy sources range in size from mega-watts to milli-watts

Mega watt generators	Milli watt generators	Nanotechnologies
		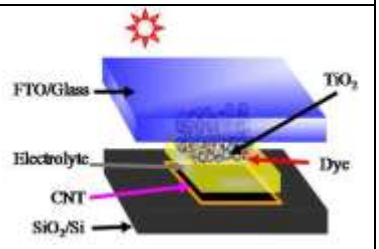
1: 500MW Nellis AFB Solar panels, Fort Irwin [2]	2: Solar cell powered calculator by Texas Instrument	3: Dye sensitive solar cell[3]
		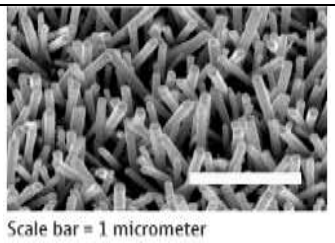
4: 5MW Offshore wind-farm on Thornton bank, Belgium [4]	5: Vibration powered wrist watch, courtesy of Seiko [5]	6: ZnO nanowire array [6]
		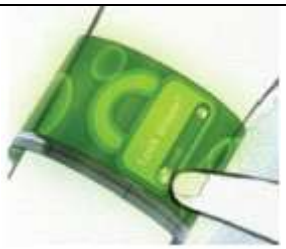
7: 22,500MW Three Gorges Dam, hydro-electric power station [7]	8: Peltier thermo electric device	9: Nokia Morph vision technology [6]

Figure 2: Energy harvesting on all scales

to micro-watts and finally nanotechnologies. Figure 2 shows the different examples that exist in each type energy harvesting and power generation. In terms of

micro and nanotechnologies the last two columns represent some of the possibilities in terms of energy production. Some applications that have already been successfully used in this technology are calculators using solar cells and the motion powered wrist watch. The solar cells in the calculators work on a photovoltaic principal which converts solar radiation into direct current electricity using semiconductors. The wrist watch on the other hand, contains a semicircular rotor that turns on a pivot depending on the wearer's movements. The movement is translated to rotor motion which through and intricate system generates electricity to keep the watch running.

These applications represent just two of many miniature devices requiring and utilizing renewable energy. One of the many reasons for the size decreases is to reduce the power consumption of these applications and in doing so allowing them to be autonomously powered. This means they would exist independent of any external power sources. The pros of using energy harvesting are vast but to name a few:

- Device lifetime is increased as compared to battery operated devices.
- Eliminates the need for any bulky connection wires and power sources.
- Maintenance is simplified and so costs are reduced
- Pollution of the environment is decreased as there is no need for ways of disposing of the chemically dangerous batteries.

Therefore it can be concluded that MEMS are a technology of the future and are going to keep shrinking and needing energy sources to match their growth. Energy harvesting of renewable energy has been found to meet this criteria but this technology will be required to shrink at the same rate as the physical sizes of the applications, yet

remain as efficient. Therefore research observing novel materials and novel methods of actuating these materials for energy generation is vital to balance this growth.

Solar energy has always received the substantial amount of attention due to it being readily available in huge quantities. Some issues have been encountered when related to properly harnessing and utilizing it efficiently. Researchers have and are working to effectively mimic the photosynthesis process of nature, which is known to be highly efficient in its use of solar energy. Some of the recent research includes Liang et al. who have been doing work on low-cost solar energy harvesting, using semiconducting polymer solar cells [8]. They utilize a polymeric composite in an attempt to overcome some previous issues like low power efficiency and improve the solar cell performance[8].

Mechanical energy is the next most widely available type of energy. From vibrations to forces and random movements, this type of energy is available in almost every aspect of daily living and can readily be converted to electrical energy using a number of different mechanisms[9]. These range from piezoelectricity to electrostatic transduction or electromagnetic mechanism. Good compatibility has been found between micro-electromechanical systems (MEMS) and the piezoelectric and electromagnetic transduction mechanism. The electromagnetic transduction mechanism is widely found in the electrical engineering sections [10-13]. These harvesting devices are found to be expensive due to being made using silicon technology. This leaves piezoelectricity as the potential cost effective method of dealing with energy harvesting.

In 1996 Starner published a paper on research done studying the use of human mechanical energy to power mobile computers[14]. The paper analyzed the generation of power through various ways including limb motion and body heat[14]. The author aimed to show that the necessity of batteries could be minimized if the human mechanical energy could be efficiently harvested and channeled. In 1998Kymissis et al, published work based on studying piezoelectric devices that could harvest excess energy and simultaneously generate electrical power, while walking[15]. These devices would be placed in the heel of a shoe, as shown in Figure 3, and then the walking motion and weight of the wearer would be the source of harvesting and power generation [16].

Figure 3: Example of the transducer in the heel of a shoe

The importance of the material used is of vital importance and is dependent on the particular application. Various piezoelectric materials have been studied and used in these different projects example: polyurea, polyamide, and liquid crystalline polymers

[16]. In terms of energy harvesting involving piezoelectric materials, a material exhibiting positive characteristics like flexibility, cost efficiency, good compatibility and high voltage output would prove to be a good fit. One such material is polyvynilidenefluoride or PVDF. This is due to PVDF showing strong piezoelectric effects, its recorded intensities are found to be around ten times larger than other polymers [16].

1.2. Historical Background of Piezoelectricity

The initial foundations of the piezoelectric property are historically related to the findings of a scientist by the name of Aepinus, in 1756 [17]. He observed and proved the electrical nature of the opposite polarities that existed between the ends of a heated Tourmaline crystal. The Curie brothers are historically responsible for the actual discovery of piezoelectricity. They announced and presented their results in 1880 at the session of the Academie des Sciences in Paris[17-18]. These experiments encompassed observing conversions of mechanical energy into electrical energy in materials like tourmaline, quartz and Rochelle salt. As interesting and mind engaging as this phenomenon was it remained dormant in use and application until the eras of the World Wars came into being. The first major use of this property was brought about in 1916 by a Frenchman named Paul Langevin[19]. The application was a sonar system or also known as an ultrasonic submarine detector. This device utilized the inverse piezoelectric effect and was made up of thin quartz crystals used for the transducer and a hydrophone as the detection unit. Therefore using the transducer to send out a high frequency signal

and measuring the time it takes to receive an echo, one could calculate the distance from the object responsible for the reflection[20].

Following this application many other projects used this principal to produce devices that would prove useful for human kind in general. Bell telephone libraries utilized this technology for multichannel telephones and other companies have focused on the designing of actuators, transducers, sensors and so on [21-23]. Early on all work was revolving around the quartz crystal and Rochelle salt so there was a need for a possible synthetic material that could provide the same effect. Barium titanate was the first synthetic piezoelectric substance produced[24]. $BaTiO_3$ was used because its capabilities where in the same ranges as Rochelle salt and it had high permittivity and good temperature coefficient.

Synthetic quartz became available 1968 and then in 1969 Kawai discovered that by applying an electric field across polyvinylidene Fluoride (PVDF) one could induce a strong piezoelectric effect within it[22, 25]. Therefore over those two years the dependence on natural crystals greatly decreased. Following this discovery, a lot of research went into observing the possibilities and capabilities of this material. This led to the discovery of pyroelectricity in polarized PVDF films by Nakamura et al. and Bergman et al. in 1971[26-27]. The uses and application of these materials now are wide and cover all sorts of specialty fields. Piezoelectric crystals are found in microphones, cameras, cigarette lighters and medical devices just to name a few [20-22].

1.3. Basics of Piezoelectricity

The root of the word “piezo” is the Greek word “piezein” which means to squeeze or to press. Therefore piezoelectricity would translate to electricity from squeezing or pressing. In more scientific terms piezoelectricity is the property of a material to produce a voltage due to mechanical stress[18]. The electric responses can be observed and measured in a number of ways, depending on testing methods and equipment. The basis of the electrical responses can be attributed to the stress on the electrode area and the applied mechanical strain on the material. There are constitutive equations relating these parameters within a material and these can be identified using a tensor notation and labeling the axes as shown in Figure 4.

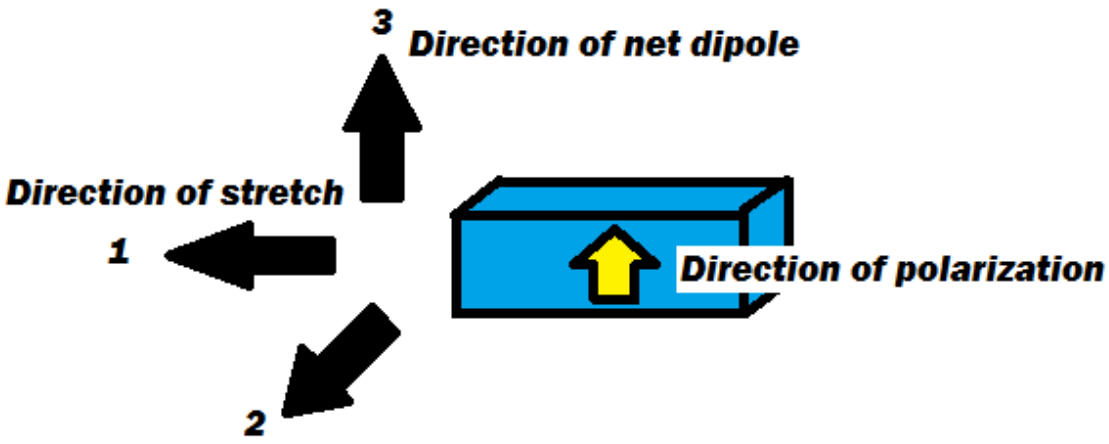

Figure 4: Tensor directions used for derivation of constitutive relations

Axis 1 represents the stretch direction; axis 2 is orthogonal to axis 1 while axis 3 shows the polarization axis. The net dipole moment lies along the polarization axis. The shear planes would be represented by 3 axes 4, 5, 6 which lie perpendicularly with respect to the first three axes.

The piezoelectric property is a combination of different effects, Hooke's law and the electrical behavior of the material[16, 18]. Hooke's law is represented by the following equation S=s*X, where S represents strain, s represents compliance and X represents stress. The equation related to electrical behavior is D=ε*E, where D represents volumetric charge density, ε represents permittivity and E represents electric field strength[16]. It is the combination of these two effects that embody the piezoelectric property. These equations are used in combination to provide two equations coined coupled equations[18, 22]. These equations look as follows:

$$\{S\} = dE + S^{E}X$$

$$\{D\} = \varepsilon^{X}E + dX$$

where the meanings of the symbols are as follows:

- d is the piezoelectric strain constant
- superscript E indicates a zero, or constant, electric field
- the superscript X indicates a zero, or constant, stress field

These coupled equations can be expanded and written in matrix form, as shown in Figure 5, to express the strain-charge form.

$$\begin{vmatrix} S_1 \\ S_2 \\ S_3 \\ S_4 \\ S_5 \\ S_6 \end{vmatrix} = \begin{vmatrix} d_{11} & d_{12} & d_{13} \\ d_{21} & d_{22} & d_{23} \\ d_{31} & d_{32} & d_{33} \\ d_{41} & d_{42} & d_{43} \\ d_{51} & d_{52} & d_{53} \\ d_{61} & d_{62} & d_{63} \end{vmatrix} \begin{vmatrix} E_1 \\ E_2 \\ E_3 \end{vmatrix} + \begin{vmatrix} s_{11}^E & s_{12}^E & s_{13}^E & s_{14}^E & s_{15}^E & s_{16}^E \\ s_{21}^E & s_{22}^E & s_{23}^E & s_{24}^E & s_{25}^E & s_{26}^E \\ s_{31}^E & s_{32}^E & s_{33}^E & s_{34}^E & s_{35}^E & s_{36}^E \\ s_{41}^E & s_{42}^E & s_{43}^E & s_{44}^E & s_{45}^E & s_{46}^E \\ s_{51}^E & s_{52}^E & s_{53}^E & s_{54}^E & s_{55}^E & s_{56}^E \\ s_{61}^E & s_{62}^E & s_{63}^E & s_{64}^E & s_{65}^E & s_{66}^E \end{vmatrix} \begin{vmatrix} X_1 \\ X_2 \\ X_3 \\ X_4 \\ X_5 \\ X_6 \end{vmatrix}$$

$$\begin{vmatrix} D_1 \\ D_2 \\ D_3 \end{vmatrix} = \begin{vmatrix} \varepsilon_{11}^T & \varepsilon_{12}^T & \varepsilon_{13}^T \\ \varepsilon_{21}^T & \varepsilon_{22}^T & \varepsilon_{23}^T \\ \varepsilon_{31}^T & \varepsilon_{32}^T & \varepsilon_{33}^T \end{vmatrix} \begin{vmatrix} E_1 \\ E_2 \\ E_3 \end{vmatrix} + \begin{vmatrix} d_{11} & d_{12} & d_{13} & d_{14} & d_{15} & d_{16} \\ d_{21} & d_{22} & d_{23} & d_{24} & d_{25} & d_{26} \\ d_{31} & d_{32} & d_{33} & d_{34} & d_{35} & d_{36} \end{vmatrix} \begin{vmatrix} X_1 \\ X_2 \\ X_3 \\ X_4 \\ X_5 \\ X_6 \end{vmatrix}$$

Figure 5: Strain-charges of coupling equations

The piezoelectric strain constant d, the permittivity ε and the material compliance s are defined as a result of the equation coupling. When looking at the coefficient d_{11} for example, the direction of the electric field is represented first subscript, while the stress or direction of deformation is represented by the second subscript. Some other important piezoelectric properties are the voltage constant g, the stress constant e and the strain constant h. The relations between these constants are found in the electrical and mechanical properties of the material [16, 22]. Table 1 presents the equations for the above mentioned constants [17]. The first equation presents the direct piezoelectric effect while the second shows the converse piezoelectric effect.

Table 1: Piezoelectric constants and their definitions

EQUATIONS	UNITS
$d = (dD/dX)_E = (dS/dE)_X$	(C/N or m/V)
$e = (dD/dS)_E = -(dX/dE)_S$	(C/m or N/Vm)
$g = (dE/dX)_D = (dS/dD)_X$	(Vm/N or m^2/C)
$h = (dE/dS)_D = -(dX/dD)_S$	(V/m or N/C)

Polarization is a very common term when studying piezoelectric materials. It is directly related to the piezoelectric constants and refers to the degree of piezoelectricity of the material. A change in polarization within a piezoelectric material comes as a result of an applied stress or strain, in constant temperature and zero electric field[16, 18]. As we've seen these material are anisotropic and so polarization will be represented by a vector with components in directions 1,2 and 3[16]. Therefore in returning to the relation between the piezoelectric constants and polarization, the relating equations will look as follows:

$$\Delta P_i = d_{ij} X_j$$

$$\Delta P_i = g_{ij} S_j$$

As mentioned above the direction of the electric field is represented first subscript, while the stress or direction of deformation is represented by the second subscript.

1.4. Polyvynilidenefluoride

Better known by its acronym PVDF, Polyvynilidenefluoride is a semi-crystalline thermoplastic polymer is part of the fluoropolymer family. PVDF has been observed to be a strong material, its recorded glass transition temperature and melting point are -40^{o}C and 150^{o}C respectively [28]. When properly orientated this material exhibits piezoelectric and pyroelectricproperties. Due to these favorable properties, Engineers and designers have used PVDF in creating an array of applications varying from sensing devices and actuators to piping and insulation products. $(C_2H_2F_2)_n$ is PVDF's chemical formula and its monomer is represented in Figure 6.

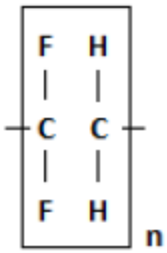

Figure 6: PVDF monomer

Addition polymerization which is sometimes known as chain reaction polymerization is the general method used to produce this material. The process takes place in a reactor where pressure and heat are used to break double bonds that exist between unsaturated repeat units. Once loose these broken bonds proceed to link up and form a chain[28-29]. These chains prefer to exist in a position where their potential energies are minimized and so they position themselves in torsional bonds. This positional setup has substituent groups which are called gauche g and transor t.

The gauche setup is realized when there is a 60^{o} angle between the substituent groups while the transor setup is observed when a 180^{o} angle is the groupd separating angle[30-31]. The length of the formed chains plays an important role in determining the formation and properties that will exist in these polymers. Due to the difficulty attributed to the accurate determining of these lengths, the materials molecular weight has been accepted by polymer scientists as a good indicator of the chain lengths. A direct proportionality was drawn which related an increase in molecular weight to an increase in chain length[28]. Another relation showed that with increase in length there was an increase in material viscosity due to an increase in entanglements.

PVDF has been observed to possess four major phases (crystalline Polymorphs): Beta (β) phase, Alpha (α) phase, Gamma (γ) phases and Delta (δ) phase. Particular attention is given to the Beta phase. This phase which is showed in Figure 7A is the phase responsible for housing the piezoelectric property. It has been observed to have an all-transor conformation (TTT) with small 7^{o} deflections along some of the monomers [30-32]. This conformation has all the dipoles pointing in a common direction, its chain axis is normal to its chains and so is known as a non-centrosymmetric, highly polar crystal.

The most prominent phase shown in Figure 7B, is called the Alpha phase. This phase is observed to be made up of a trans-gauche-trans-gauche (TGTG) conformation. Contrary to what is observed with the Beta phase, the Alpha phase shows a centrosymmetric, anti-polar setup[29-30].

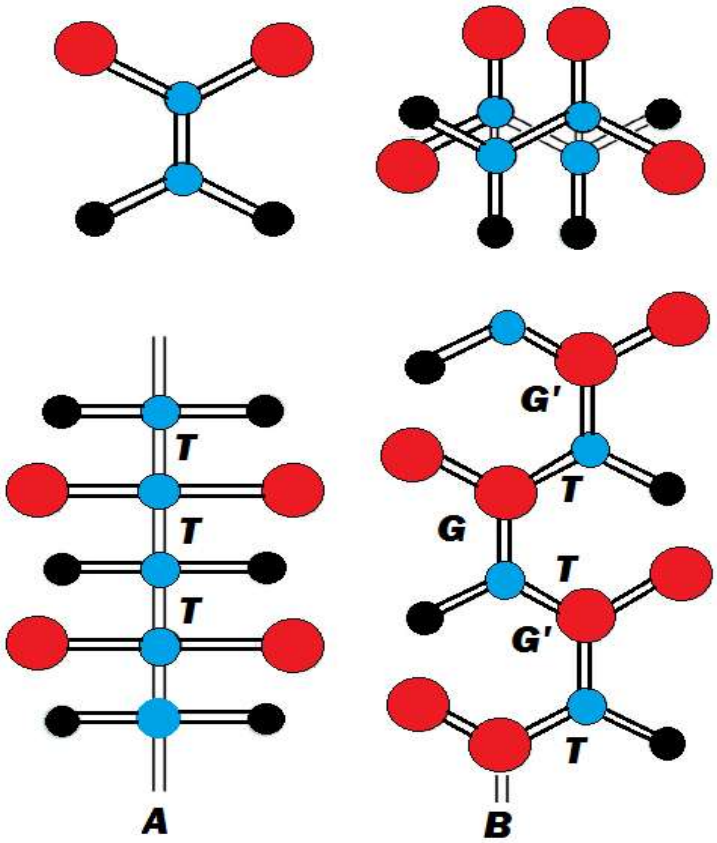

Figure 7: A--- beta phase B--- alpha phase

The next phase discussed is the Delta phase. This phase is also known as the Alpha poled form. This is due to the two phases having the same conformation yet in the case of the Delta phase every second chain experiences a rotation and an alignment. This change in its conformations makes the Delta phase a polar non-centrosymmetricphase[30-32]. The last phase has a non-centrosymmetric setup and is called the Gamma phase. It is observed to have a T3GT3G' configuration with all its chains positioned parallel to each other[32-33].

1.5. Fe_3O_4 Magnetite

Magnetite is a naturally occurring magnetic ferromagnetic mineral. Its chemical formula is Fe_3O_4 and it represents one of a number of different existing iron oxides. Magnetite's is a widely used filler material when working with polymers, due to its good magnetic and electrical properties [34]. These have allowed for their composites to be used in a range of applications from medical applications to recording media [35-36]. A lot of research has been done to study not only the characteristics of this material but also its functions as a filler material in polymer samples. Apart from just its magnetic property, this material has the magnetostriction property. Magnetostriction refers to the materials experiencing a change in dimension as a result of being placed in a magnetic field.

Wei et al.[37] characterized hyper-branched aromatic polyamides/ Fe_3O_4 magnetic nano-composite, by examining the composites behavior within an applied magnetic field. Razzaq et al. [34] studied various properties of the shape memory polymer, PU. Qiu et al.[38] focused on the synthesis of Polyaniline/ Magnetic iron oxide nano-composite using Ultrasonic Irradiation, after which they studied the magnetic properties and surface morphology. All this research has greatly increased the understanding and knowledge of this material within common polymers. However none of these studies focused on how this material would act and affect the piezoelectric properties of a polymer. Incorporating these characteristics with those of the piezoelectric PVDF would provide a functional composite with a broad range of vary useable characteristics.

CHAPTER II

MOTIVATION AND OBJECTIVES

As discussed in Chapter I, there is a growing demand in MEMS technology and a need to find energy sources to match the growth. Energy harvesting of renewable energy has been found to meet this criteria but this technology will be required to shrink at the same rate as the physical sizes of the applications. Therefore it is important to develop new materials that can have improved properties and characteristics to meet these demands. In regard to piezoelectric harvesting devices, the majority of emphasis is placed on electromechanical activation. Improvement in the performance of these materials and incorporating new methods of activation would open the door to numerous possibilities in terms of inventive applications and research.

This research aims to incorporate magnetic particles in a piezoelectric polymer, with the vision of improving the material's performance and adding another dimension of activation. Successfully synthesizing a composite of a piezoelectric polymer and a magnetic material would provide an interesting functional material. This composite material could find a use in energy harvesting, battery technology, drug targeting, cell separation and electro-rheological fluids. The two materials proposed for use in this research are Polyvinylidenefluoride and Fe_3O_4 (Magnetite) Nano-particles. Research will focus on the synthesis and characterization of the proposed material. The synthesis process will aim to provide a simple, repeatable, and efficient manner of producing the samples. The synthesis process includes the following steps: Melting of the PVDF

pellets; Measuring and separation of particles and corresponding PVDF solution; Dispersion and mixing of particles into PVDF solution; Thin film spin casting; Corona poling process.

The characterization includes using these techniques: X-ray diffraction; optical microscopy; Atomic force microscopy; Dynamic mechanical analysis; and a linear stage.

The research is expected to obtain understanding in the materials developed. Characterization techniques allow for the examination of the microstructure, the morphology, the interaction, the modulus, the piezoelectric properties and some thermal properties as well. A better understanding of the material will allow for looking into possible applications, granted the material functions correctly.

CHAPTER III

EXPERIMENTAL

This chapter introduces the materials and experimental procedures that were followed in the proceedings of this research. It encompasses the synthesis and characterization processes that were used to study the composite material. The chapter begins with the introduction of the materials used to produce the composite. It is then followed by the sample preparation technique. The following section covers the thin-film casting method and the corona poling process.

3.1. Materials

The materials used in this research were Polyvinylidenefluoride (PVDF) and nanometer sized Fe_3O_4Iron Oxide (II, III) {<100nm}. The individual properties of these materials are the main factors for the choice to use them in this research. PVDF is a piezoelectric polymer and Fe_3O_4 is a naturally occurring magnetic mineral. Some important properties of both materials are summarized in Tables 2 and 3.

Table 2: Selected properties of PVDF

Properties	Values
Chemical Formula	$CH_2 = CF_2$
Glass Transition Temperature	-38^oC
Melting Temperature	160^oC
Thermal Conductivity	0.719 m/K
Heat Capacity	13.59 cal/mol

Table 3: Selected properties of Fe3O4

Property	Value
Chemical Composition	Fe_3O_4
Chemical Classification	Oxide
Characteristics	Strongly magnetic, black color, octahedral crystal
Thermal Conductivity	9.7 W/m K
Form	Spherical Nanopowder
Surface Area	BET surf. area >60 m^2/g
Particle Size	<50 nm (TEM)

The PVDF was purchased in pellet form from Sigma Aldrich. This polymer was chosen due to the majority of its positive characteristics including its piezoelectric

properties, its flexibility and availability. Nano-Fe_3O_4Iron Oxide (II, III) was used as the nano-particles in the composite. Also known as magnetite, Fe_3O_4 is a naturally occurring magnetic black iron core. These nano-particles were purchased from Sigma Aldrich. The reagents used in the synthesis were dimethylsuphoxide (DMSO) and acetone, which were both purchased from Sigma Aldrich. Figure 8 shows the packaged materials used in this experiment.

Figure 8: PVDF and magnetite containers

3.2. Material Synthesis

The granular PVDF pellets, shown in Figure 9, were measured out in a batch of 5g. The pellets are placed in a solution containing 80ml of acetone and 20 ml of DMSO.

Figure 9: PVDF pellets

This mixture was then placed on a hotplate at a 35°C-40°C, and a stirrer is added into the solution to increase the dissolving rate. The melting setup is shown in Figure10. The stirrer aids the dissolving process by adding a disturbance to the mixture. The stirrer should be removed after 30 minutes once the PVDF pellets begin to deform and melt on each other. The heating process, while melting the PVDF, causes the DMSO and acetone to evaporate.

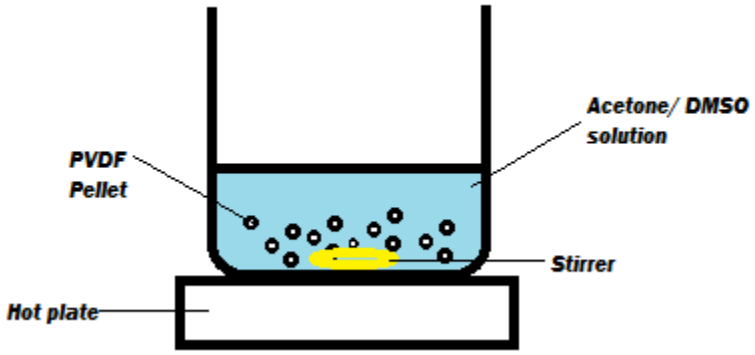

Figure 10: Sample preparation setup

The viscosity of the final solution depends on how fast or how slow this evaporation moves, therefore depending on desired solution thickness, the temperature can be adjusted accordingly. The process will take between 60-100 minutes till completion.Once the pellets are fully dissolved the solution will appear clear and see-through.

3.2.1. **Particle Dispersion**

The melted solution is then poured out in equal quantities of 15mg into smaller containers. The containers were weighed before and after the solutions were poured into them, thus allowing for the knowledge of the exact weight amount of solution. The nano-particles were then weighed out in the following weight ratios of solution to particles as shown in Table 4.

Table 4: Sample ratios

PVDF	Fe_3O_4
100%	0%
98%	2%
93%	7%
88%	12%

The particles were then dispersed within the corresponding containers. The mixture was then placed in a mixer and set to mix for2 hours. Figure 11 shows what the final mix product would look like.

Figure 11: Melted PVDF/Fe3O4 solution

3.2.2. **Film Casting**

The PVDF/Fe_3O_4 solutions were then spun into thin films using the Laurell WS-400B-6NPP Spin coater shown in Figure 12. The films were spun upon a 484 mm^2 microscope disks. A drop (approximately 10 mm) of the selected solution was placed onto the microscope disk using a standard pipette, and then spun to a thin film. All films were spun at identical speeds and cycles. These cycles ran as follows 500rpm – 1000rpm – 500rpm, with each cycle running for 10 seconds. After the films had been spun, they were rinsed off with de-ionized water to remove any solvent possibly still on the sample. Long applications of de-ionized water have been observed to cause buckling of the sample, therefore only short application times should be used. The samples were then left to dry at room temperature for a 24hr period, further allowing for the evaporation of any solvent still left in the mixture.

Figure 12: Spin coater and sample PVDF film

3.2.3. **Corona Poling**

The piezoelectricity of PVDF depends largely on the presence of the β phase within the material. After the sample has been spun into a film, they exist primarily in

the α-phase, therefore they must be poled in order to induce the β phase and in doing so, the piezoelectric characteristics[39]. The process used to induce these characteristics is called the Corona poling process[40]. In this process an electric field was introduced between a wire carrying a high voltage and a grounded plate[40]. The polymer chains of the samples are oriented due to this high electric field and it's this orientation that brings about the piezoelectric properties. Figure 13 shows the device used to bring about this orientation.

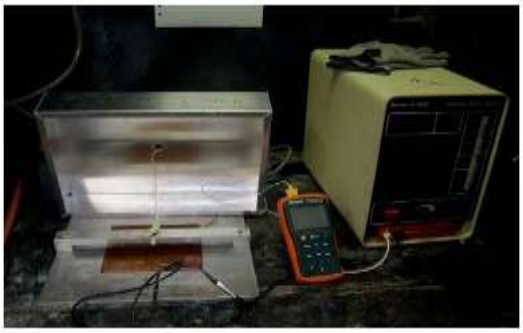

Figure 13: Corona poling setup

3.2.4. **Corona Poling Process**

Once dried a batch of the films were poled using in situ corona poling setup, illustrated in Figure 13. The film was placed beneath the conducting needle, as shown in Figure 14, and on top of the heating pad and then the top of the poling unit was closed. The temperature was then raised by adjusting the power to the heating pad by using the variable transformer. The transformer was set to 70% position, which is related to 70%

of the standard 84 V electrical outlet. From the attached VMR thermocouple reader, the temperature was monitored till it was stabilized at 140^{o}C. Once stable, the 1kV voltage source was switched on and the variable transformer was slowly returned to zero setting. This allowed the poling and simultaneous cooling of the film to room temperature, permitting the polymer chains to "freeze" in a poled or β phase position. Once the sample was returned to room temperature the voltage source was then turned off.

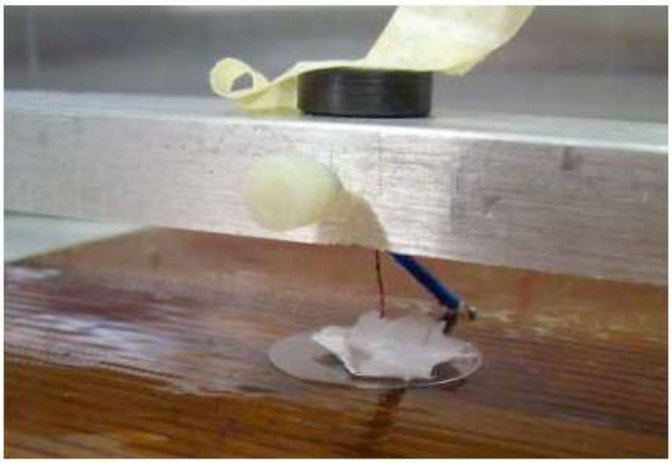

Figure 14: Poling needle on corona poling setup

3.2.5. **Conductivity Coating**

The PVDF samples exist as insulators therefore to be able to detect the electric field produced, it needs to be coated with a conductive material. Various methods exist for coating purposes: metallic inks, thermal evaporation and sputter coating. For this study sputter coating method was utilized due to availability. A Technics Hummer II sputter coater was utilized. The coating was a Gold and Palladium film of 100nm in

thickness. It was important to avoid any short circuiting of the two sides of the sample, which would not permit for any readings to be obtained. Therefore prior to coating care must be taken to avoid sizeable holes and pores through which the coating could seep. During the coating process the edges were protected and left uncoated in order to avoid any possible short circuiting.

3.3. Characterization

This section will focus on the various methods utilized to characterize the PVDF/Fe_3O_4 composite. These methods will be explained and then the resulting data from testing the composite will then be analyzed.

3.3.1. Optical Microscopy

Optical microscope (Keyence VHX-600K) was used to obtain morphological information on a macro scale. The particle dispersion was observed and this technique also allowed for viewing the manner in which the particle settled into the polymer matrix. The transmitting mode was used on the microscope with a magnification of up to 200X. This allowed for visual differentiating of the different samples, since any greater magnification made all samples appear the same. The microscope used in this experiment is illustrated in Figure 15.

Figure 15: Keyence VHX-600K

3.3.2. **Fourier Transform Infra-Red Spectroscopy**

Fourier transform infrared spectroscopy abbreviated FTIR, is an analysis method that is used to obtain the infrared transmittance or absorption spectrum and also measures photoconductivity and emissions. The different bonds within a material react uniquely differently to other bonds after they interact with the infrared light. These differences are taken as an output and this raw data is converted to the FTIR outputs we analyze, using the FTIR methods. This tool is used to aid in assessing if we have any interactions between the polymer and the magnetic particles within it. Figure 16 presents what an FTIR output looks like. This particular image is the FTIR output for a polycarbonate sample.

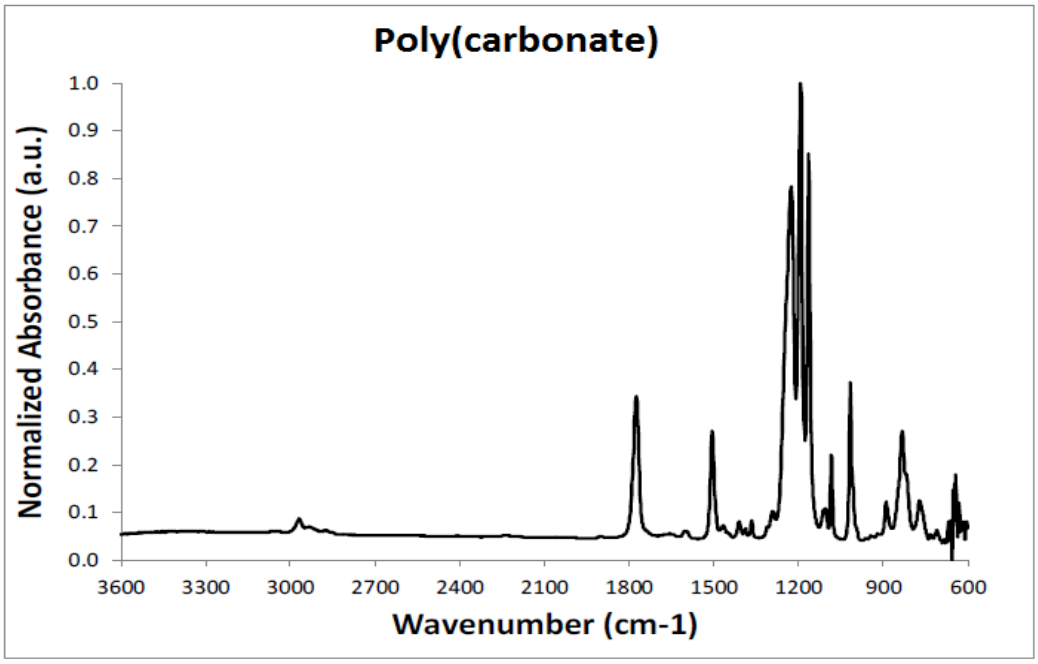

Figure 16: FTIR polycarbonate output

3.3.3. **Atomic Force Microscopy**

Atomic force microscopy (Nano-R, Pacific Nanotechnology Inc., USA) was utilized to assess the surface topography of the samples. The AFM measures the chemical, Van der Waals, electrostatic, and magnetic-dipole forces between the tip and the surface therefore providing information about the topography of the surface [41-42]. The AFM measures the cantilever deflection as it scans the surface as illustrated in Figure 17. This is accomplished by detecting the reflected laser light from the cantilever.

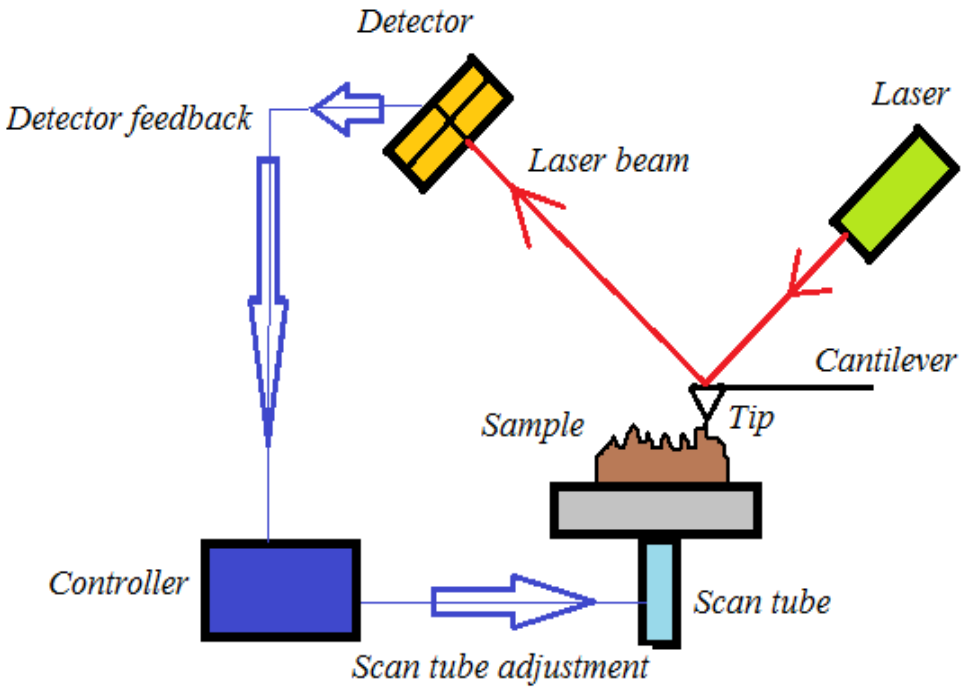

Figure 17: Example of AFM process and setup

The resolution of the AFM depends greatly on the shape and size of the tip. AFMs are now available to test at ambient conditions, under liquid environments, and with ultrahigh vacuums where the test environment depends on the application and/or the required resolution [41-43]. The AFM has two operation modes: contact and non-contact. The contact operates by placing the tip in direct contact with the sample and dragging it across the surface. This method provides a good image of the surface yet it reduces tip life due to wear. In addition it does not allow for the differentiating between materials. The other commonly used method is called the close contact method or mode. In this method, the stiff cantilever is oscillated with amplitudes between 10 and 100 nm

close to the surface at its natural frequency, so that the tip taps the surface. This eliminates friction between the tip and surface, therefore extending the lifetime of the tip. This mode is well suited for samples with poor adhesion to the substrate. The AFM used in this research was the Nano-R Pacific and it is illustrated in Figure 18.

Figure 18: Nano-R Pacific Atomic force microscope

3.3.4. **X-ray Diffraction**

X-ray diffraction (XRD) is a non-destructive characterization technique used to analyze and extract information regarding a materials crystallographic structure and chemical composition [44-46]. Diffraction refers to the interference of waves as they pass through an object. An X-ray is an electromagnetic radiation with a wavelength of between 0.01 to 100nm depending on the source [44-45]. The technique is based on elastic scattering of crystalline and semi-crystalline structures. An incident X-ray beam of known wavelength is directed towards the material being tested; when the X-ray finds an obstruction (atom) it is reflected from the material. When the object is highly oriented (crystallized), the scattered waves interfere with one another and are added and directed

with a specific orientation, this is called constructive interference [44-46]. The orientation angle from the surface is equal to the incident angle or $\theta_{in} = \theta_{out}$. Diffraction occurs where the X-ray encounters obstacles which are equally distanced, with spacing similar in magnitude to the wavelength and have the ability to scatter the wave. X-rays possess wavelengths which are about the same size as the diameter of an atom or equal in length to the distance between atoms within a solid. Therefore the X-rays are refracted when directed at solids with crystalline structures. This technique is based on the principal of Bragg's law[21, 44], which can be illustrated as shown in Figure 19.

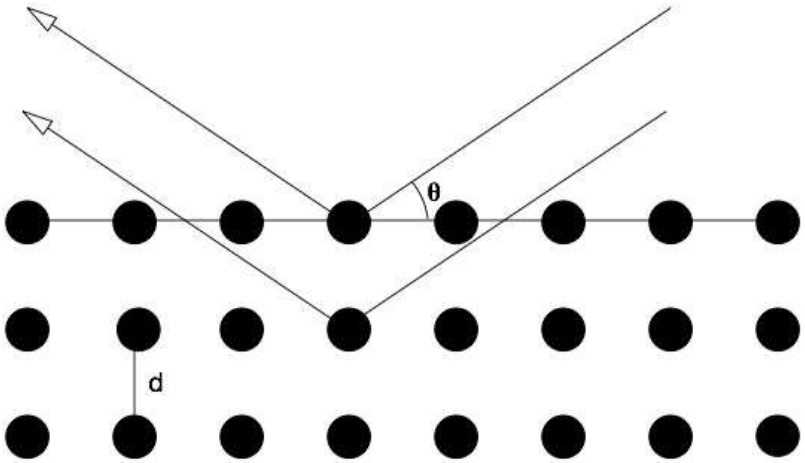

Figure 19: Example of diffraction within a crystal

$$n\lambda = 2d \sin\theta \tag{1}$$

where n represents the order of reflection, λ represents the X-ray wavelength, d represents the distance between the parallel crystal lattice planes, and θ represents the angle between the X-ray incident beam and a particular crystal lattice

plane[44].Therefore by varying the theta angle Bragg's law is used to plot the intensities and their corresponding angular positions, with each output being particular or unique to every material.

X-ray diffraction (XRD) allowed for the observation of thecomposite thin film microstructure. Observations were made of the crystalline phases within the un-poled and poled composite thin films. The X-ray diffractometer (D8 Advance Bragg-Brentano, BrukerAxs Inc., USA) was used to observe the structural characteristics of the prepared samples. The scans were performed with the 2θ angle ranging from 10 to 70° and a step size increment of 0.15°. This allowed for good resolution on the diffraction outputs which were then analyzed using X-ray diffraction program MDI-jade.

3.3.5. **Dynamic Mechanical Analysis**

Dynamic Mechanical Analysis or DMA, is a technique that allows the retrieval of material transitional properties as a result of applied stress. Small deformations are applied to the material at a set frequency while the temperature is changed, and the materials response is monitored. This technique allows for the acquisition of the glass transition temperature, melting temperature, storage and loss modulus amongst other things [47]. Figure 20 shows the transitions that exist within a polymer when its temperature is raised. The tansition temperatures and the material modulus offer a lot of information when it comes to understanding a materials behaviour. The DMA test will allow for the gathering of such information regarding the PVDF/Fe_3O_4 samples.

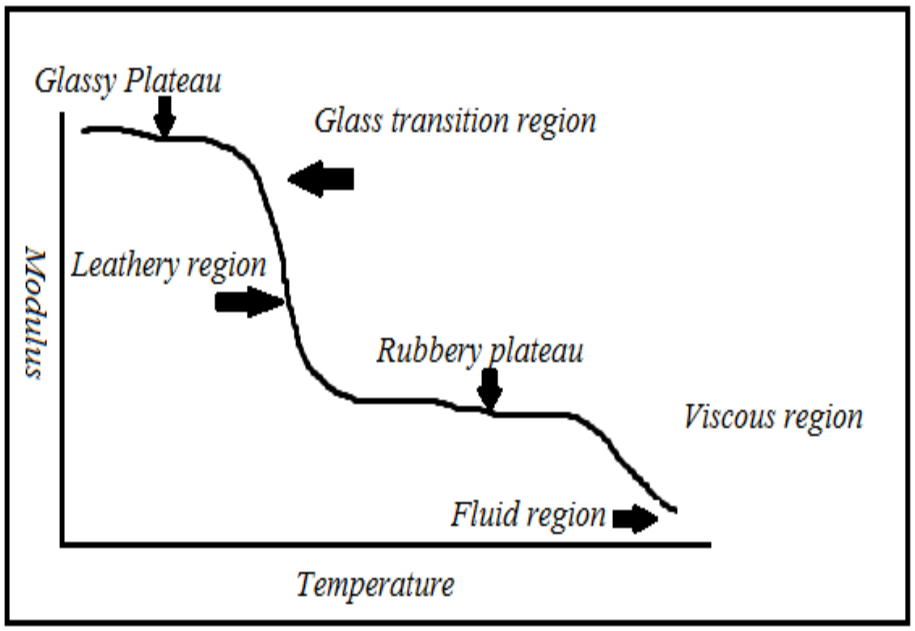

Figure 20: Polymer modulus vs. temperature

This test was run on a TA Instruments Q800 DMA. The parameters used are shown in Table 5.

Table 5: DMA testing parameters

Temperature range	
Ramp	5 C^0/min
Frequency	1Hz
Amplitude	10 microns

3.3.6. **Differential Scanning Calorimetry**

Differential Scanning Calorimetry often known by its acronym DSC, analyzes thermal properties of a material. This technique measures the difference in quantity of the heat that is needed to raise the sample temperature as compared to the reference sample, and plots this with respect to temperature. When working with polymers this method allows for the viewing of the melting temperature, crystallization temperature and the glass transition temperature [47]. This test allowed for the observation of the thermal behavior of the sample material. There was also the acquisition of information regarding the effect the Fe_3O_4 particles would have on the characteristic thermal behavior of the PVDF sample. This is a fairly simple technique as the illustration shows in Figure 21. The sample was placed in the sample holder while the reference holder was left empty. The heaters below each pan were simultaneously switched on by the computer and they were heated at equal specific rates of $10C^0$/min. The foundations of this technique are based on the fact that when samples undergo phase transitions, they require heat to flow to it. The change observed with the sample was then compared to the reference holder behavior. No changes are expected on the reference holder. One is able to differentiate between an exothermic and an endothermic reaction due to one requiring more heat (endothermic) while the other needs less heat (exothermic).

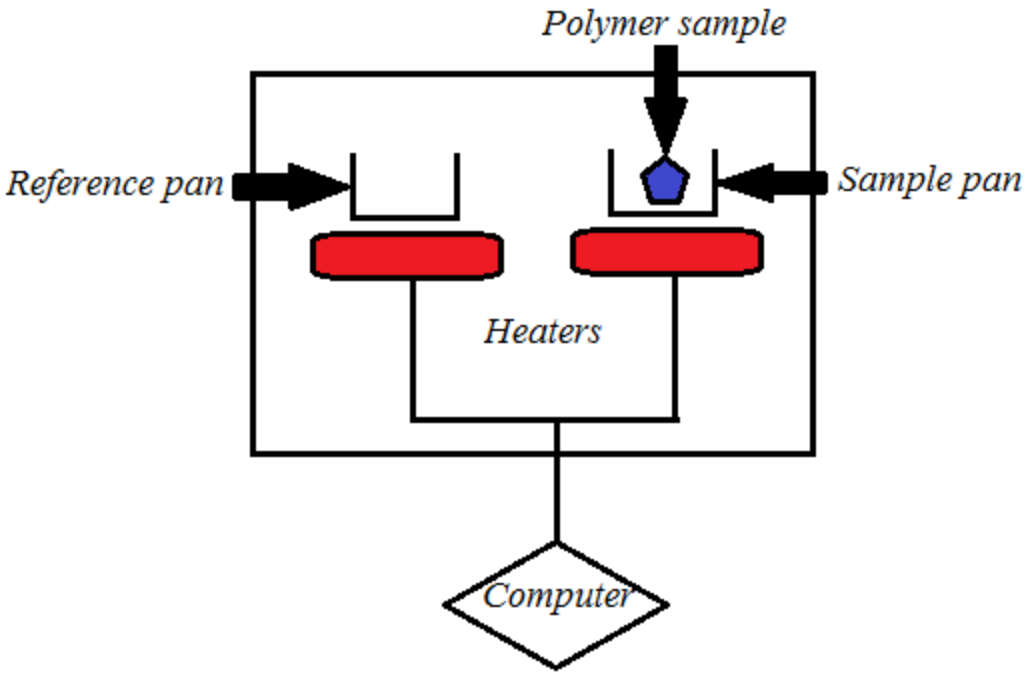

Figure 21: Differential scanning calorimetry setup schematic

3.3.7. **Linear Stage Testing**

The linear staging setup was assembled to monitor the piezoelectric output of polymer samples under dynamic bending. An illustration of the setup is shown in Figure 22.The piezoelectric property produces an output voltage during bending, stress or when placed in an electric field. Linear staging uses the bending capability, as shown in Figure 23. This setup contains one mobile and one immobile stage as illustrated in Figures 24 and 25. On top of these are the clamps for setting in the sample to be tested. This setup was connected to and operated via a computer. Lab-view programs were used which ran these tests and kept parameters set to the researcher's preferences. While running these tests two leads from the sample are connected to the computer and they allow for the

monitoring of the voltage outputs from the materials. Figure 25 shows the dimensions of this testing device as used in the experiments.

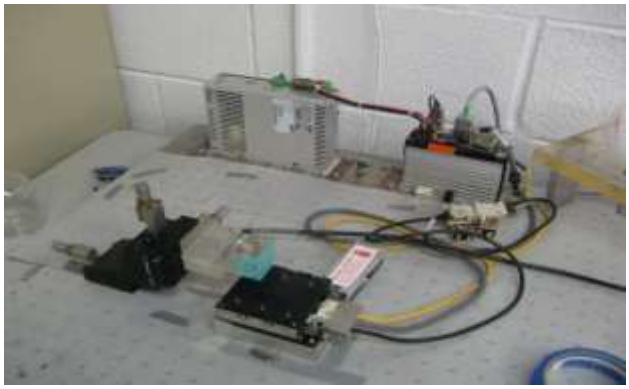

Figure 22: Linear staging setup

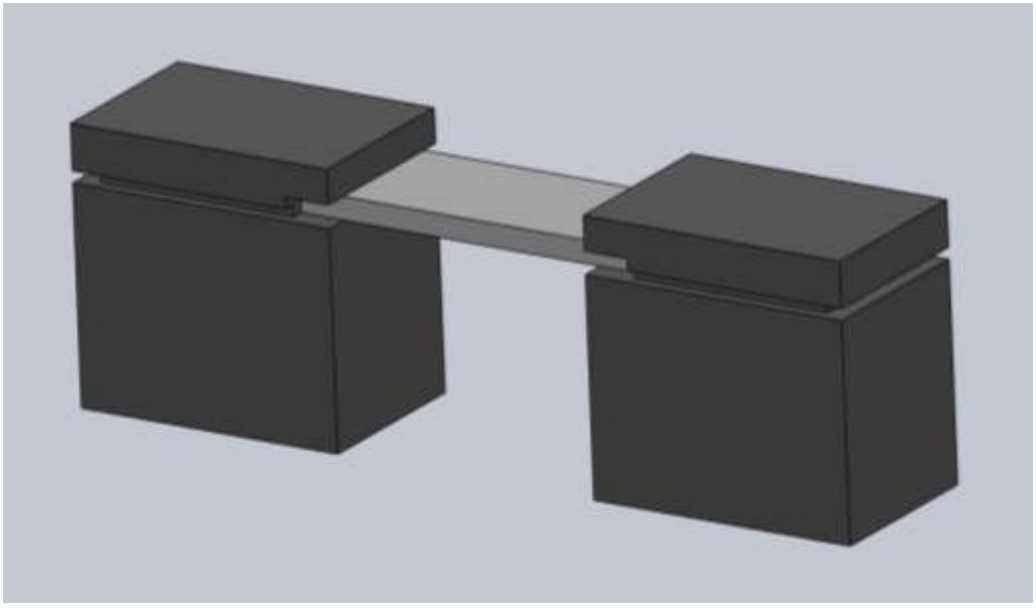

Figure 23: Pre-bending configuration

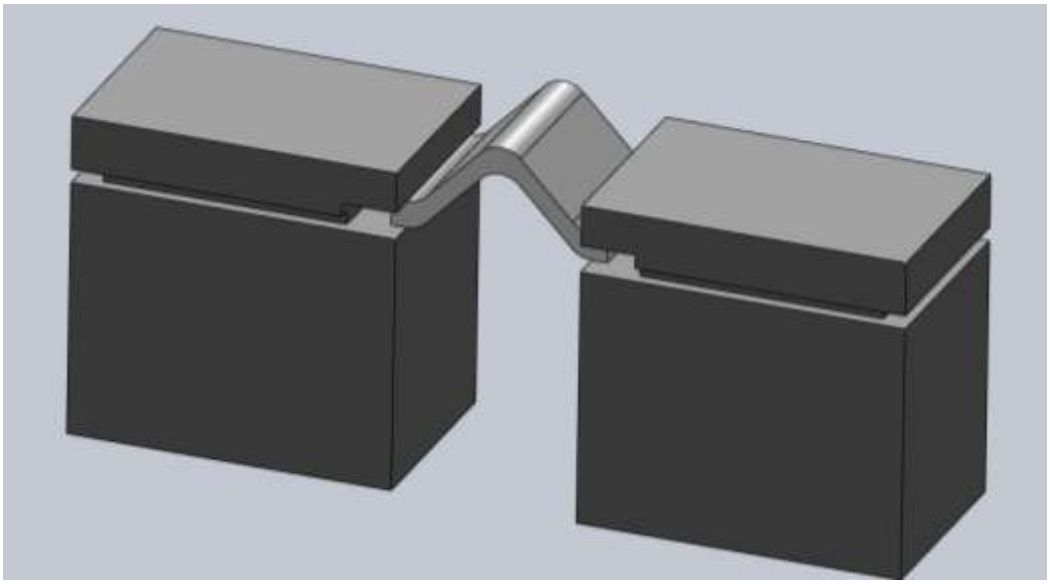

Figure 24: Post-bending configuration

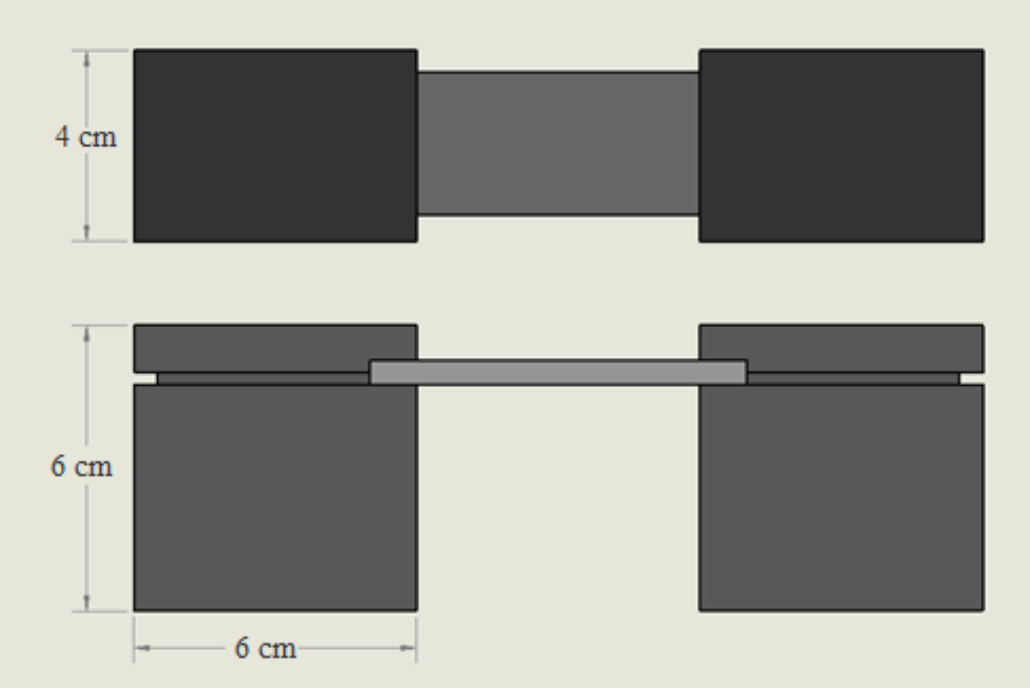

Figure 25: Linear staging setup dimensions

CHAPTER IV

PROPERTIES OF A NEW COMPOSITE MATERIAL

A magnetic-nanoparticle enhanced piezoelectric polymeric composite was developed using the previously described approach. This chapter presents their physical, mechanical, and materials properties using techniques described in chapter III. Firstly the particle distribution will be observed using the Optical microscope. This is followed by chemical bonding analysis using FTIR. Surface properties are observed using the AFM and then crystallinity and microstructure of the material will be observed using the XRD. The DMA and DSC results will conclude the chapter.

4.1. Particle Distribution

In order to evaluate the particle distribution, the samples were examined using the optical microscope and the results are as shown in Figures 26-29. The images allow for the observation of the particle position in each case and also to scope the existence of porosities of the sample surface. The particles are observed as darker spots on the lighter PVDF matrix in the background. For accurate information regarding the particles, their sizes and the dispersion, the figures were analyzed using analysis software called ImageJ.

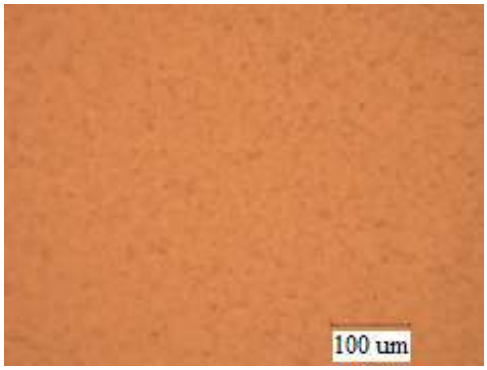

Figure 26: Pure PVDF sample

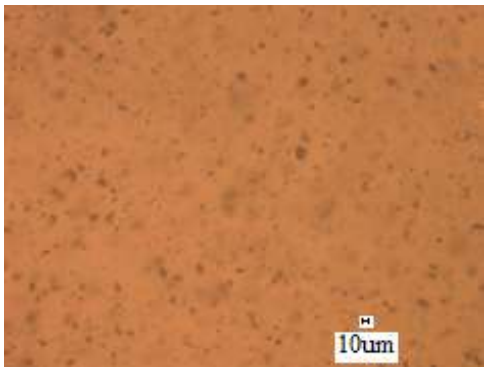

Figure 27: 2% PVDF/Fe3O4 sample

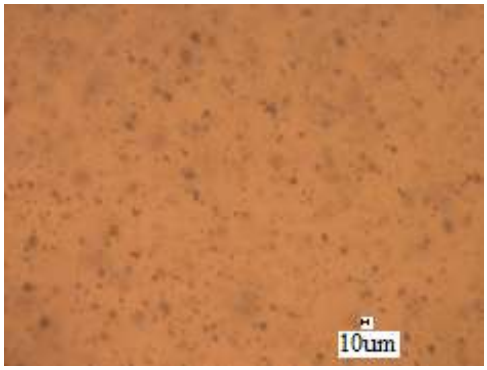

Figure 28: 7% PVDF/Fe3O4 sample

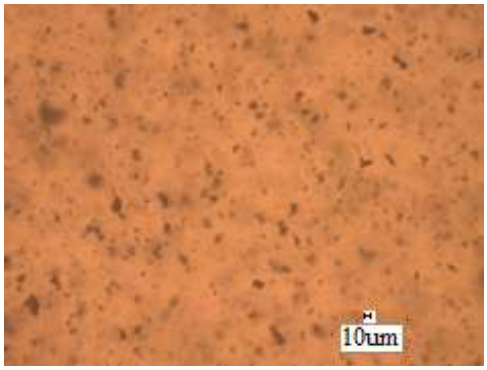

Figure 29: 12% PVDF/Fe3O4 sample

Table 6 shows measurements taken of each sample. With the increase in particles it would be expected that the amount of the covered area increases. This is shown to be the case by the first column. There appears a slight increase in the average size of the particles present, about 2um increase. For the increase in amount of particles the increase in size is minimal and this allows for an assumption of a good general dispersion.

Table 6: Particle dispersion

Sample	Percent of total measured Area	Count	Average size (um)
2%	23%	383	12.057
7%	33%	497	13.423
12%	37%	470	14.515

4.2. Chemical Bonding

FTIR was used to detect possible chemical interactions between Fe_3O_4 and PVDF. The results are shown in Figures 30 and 31.

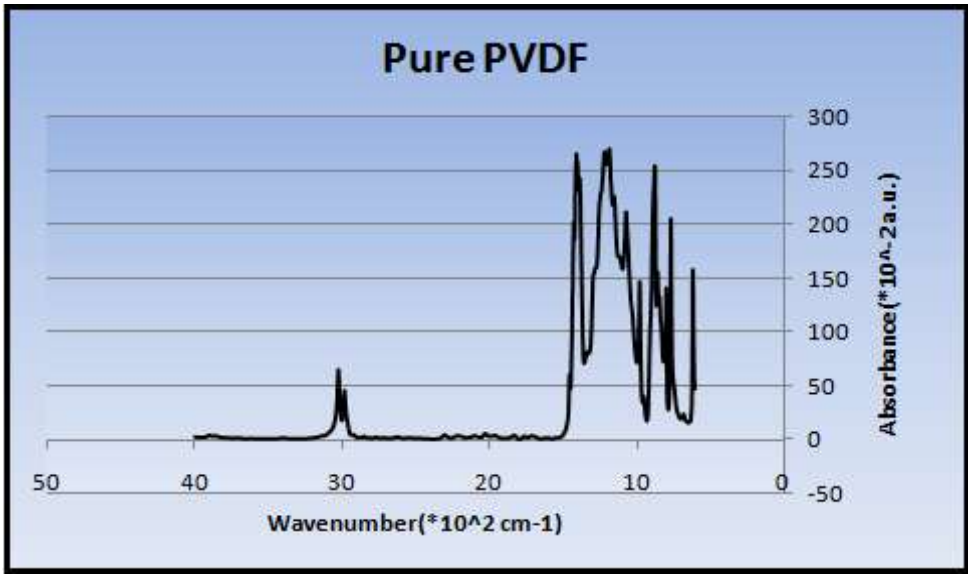

Figure 30: FTIR of pure PVDF sample

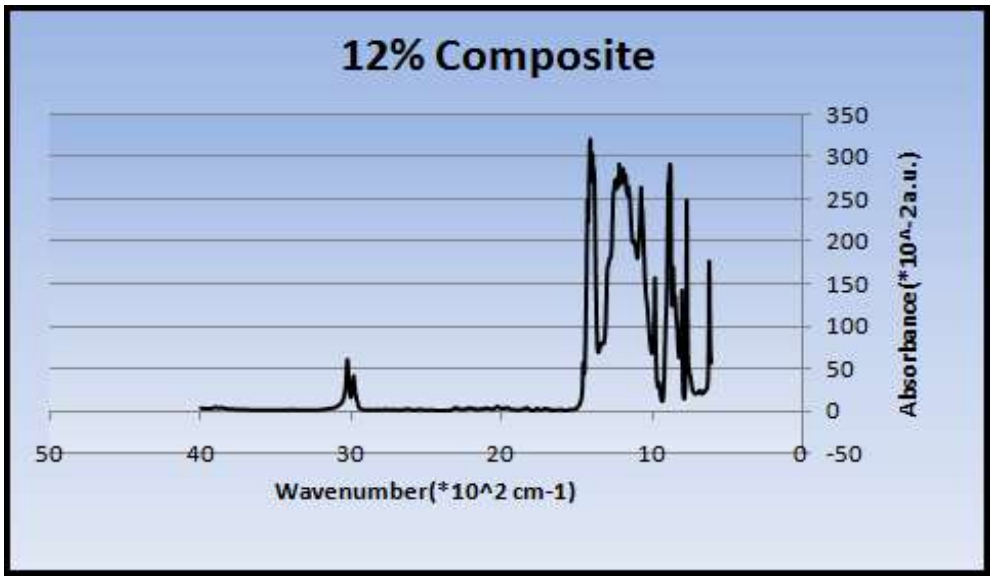

Figure 31: FTIR of 12% composite material

Chemical bonding between the PVDF and the Nano-particles would show up on the FTIR output as new peaks or shifts in the old peaks, indicating new functional groups. The result of PVDF, Figure 30, is superimposed with that of the composite, Figure 31, to observe if any changes have taken place. Figure 32 shows that there is no change and no new peaks that could indicate new bonds forming. This leads to concluding that there are no chemical bonds formed due to the addition of Fe_3O_4.

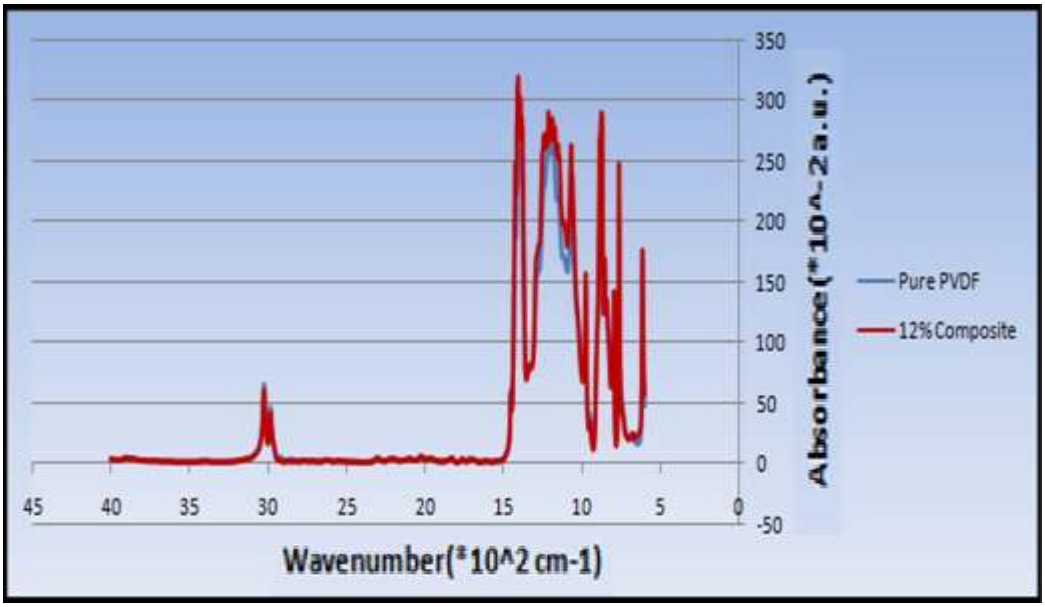

Figure 32: Superimposition of FTIR outputs

4.3. Surface Roughness and Particle Position

An atomic force microscope (Nano-R, Pacific Nanotechnology Inc., USA) was utilized to observe the surface of the various samples and the results are shown in Figures 33-36.These observations would also allow for the confirmation of the existing phases. The images are shown starting with the pure PDVF sample and then moving on with increasing Fe_3O_4 content. With these being height images the lighter shade is indicative of the higher areas of the sample. These images were analyzed using the NanoRule software, allowing for the observation of the changes in surface roughness parameters.

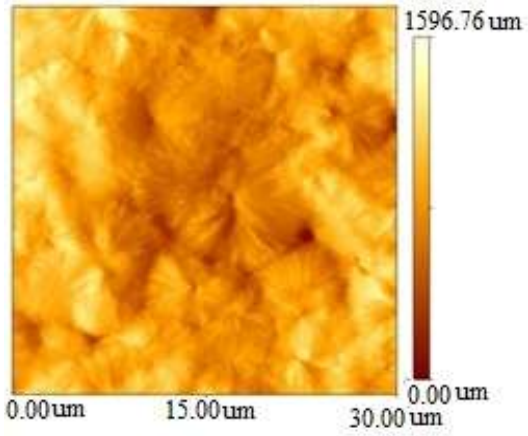

Figure 33: Surface of pure PVDF sample

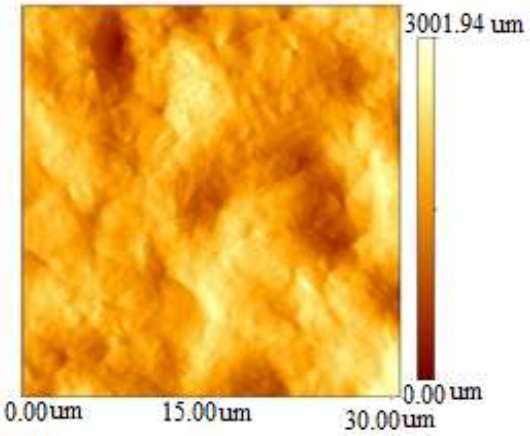

Figure 34: Surface of 2% PVDF/Fe3O4 sample

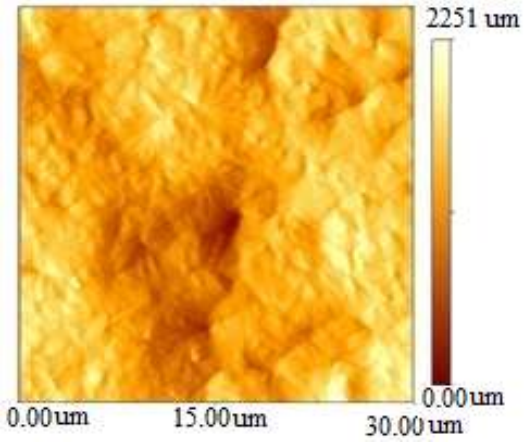

Figure 35: Surface of 7% PVDF/Fe3O4 sample

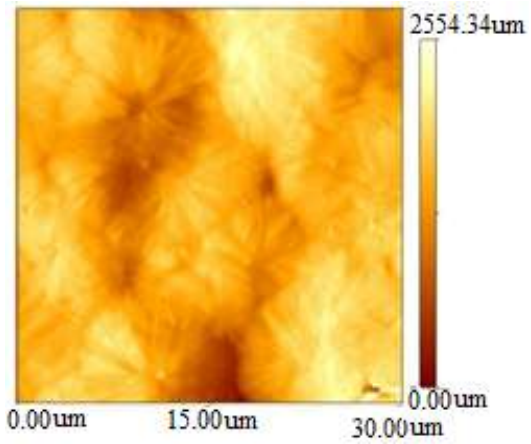

Figure 36: Surface of 12% PVDF/Fe3O4 sample

Jain et al. showed that the unadjusted surface of an β-phase sample shows grain aggregation like features[48]. These spherulitic aggregations house acicular crystallites emanating from the center. Looking at the AFM resulting images it is clear to see some of the β-phase patterns, thereby confirming the presence of the phase. Using the AFM

the surface roughness of the samples was measured and documented for comparison. The roughness results are presented in Table 7. It is observed that there is a slight modification and increase in the roughness from sample to sample, even though the observed change is minimal. This minimal change in surface roughness is attributed to the increase in the amount of particles within the samples. A substantial increase in roughness would indicate that the particles are not settling into the polymer matrix and therefore sitting on the surface. Therefore these results would infer that the particles are embedding themselves in the PVDF.

Table 7: Roughness parameters

	0%	2%	7%	12%
Total area (um^2)	907.26	907.26	907.26	907.26
Roughness Avg. Ra (nm)	235.16	301.72	317.99	320.02
Root mean square Or (nm)	290.35	371.12	393.48	412.43

4.4. Crystallinity and Microstructure

The XRD was used to observe the crystal structure of the composite and the effect of the Fe_3O_4 on the structure and phases of the material. This method has been commonly used to identify phases in polymeric materials [49-50]. Figure 37 shows the resulting XRD output images from running the tests.

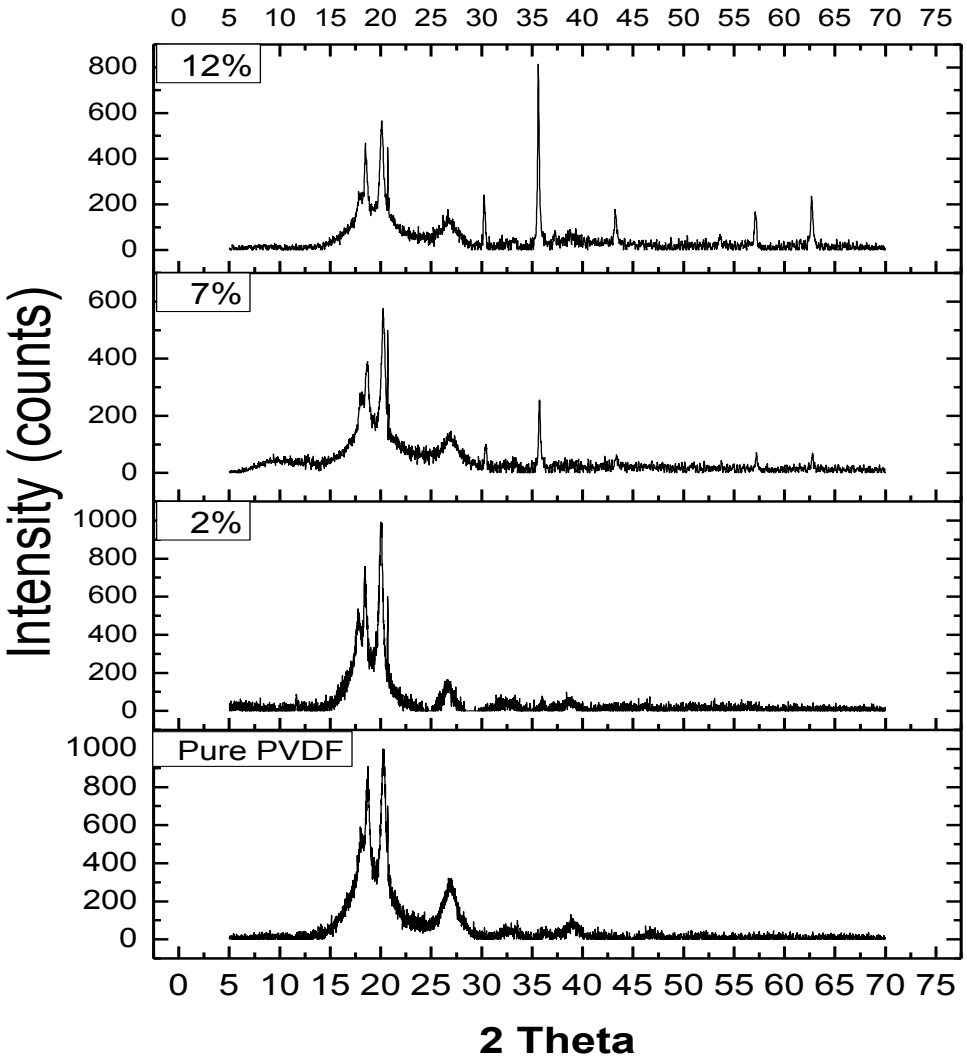

Figure 37: Diffractograms for each sample

The scans taken of the pure PVDF were compared with previous scans shown in literature and it was found to match and agree with the literature confirming our material as semi-crystalline PVDF[38, 50]. Examining the output figures of the composite, it is

observed that with the continuous increase in Fe_3O_4, there is a decrease in the intensities of the PVDF peaks. A widening of the peaks generally indicates the decreasing crystallinity in a material, yet this is not the case in this composite material. Full width at half maxima (FHWM) also plays a role in determining whether there exists a loss in crystallinity[48]. This parameter is representative of the width of the peak at the point where the peak has reached half its maximum value. The increase of FWHM means there is a decrease in the crystallinityof the material and vice versa[48]. The measured FWHM of the main peaks maintained a consistency. This means that the PVDF maintains a fairly consistent amount of crystallinity even with the increase of the particles. XRD is also a useful tool for determining the present phases within a material. As mentioned in Chapter I, PVDF exists in the alpha phase and the piezoelectric property is related to the beta phase. As a reference, some of the basic characteristic phase peaks of PVDF as mentioned in Lovinger[30] are shown in Table 8.

Table 8: Crystal phases and corresponding diffraction angles

Phase	WAXD 2θ (°)	FTIR bands (cm^{-1})
α phase	17.7, 18.4, 19.9, 27.8, 35.7, 39, 57.4	532, 612, 763, 796, 854, 870, 970, 974, 1210, 1383, 1423
β phase	20.7, 20.8, 35, 36.6, 56.1	510, 839, 1286, 1431
γ phase	18.5, 19.2, 20.1, 20.3, 26.8, 36.2, 38.7	812, 882, 1234

Using this reference the XRD outputs were analyzed for phase determination. The results are shown in Figure 38.

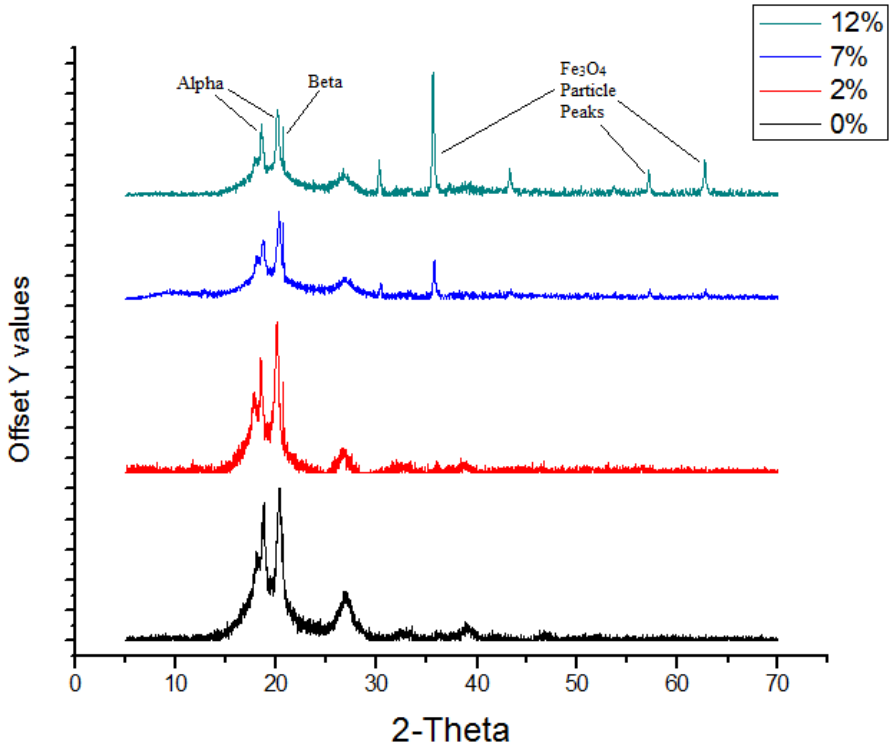

Figure 38: Peak and phase analysis

It is observed from Figure 38 that the piezoelectric possessing Beta phase is present in all samples. Even though numerous peaks attributed to these phases exist, only a couple were pointed out for ease of observation. The nano-particle peaks are seen to increase in intensity as the PVDF peaks simultaneously decrease in intensity.

4.5. Storage Modulus and Glass Transition Temperature

The DMA allowed for the testing of how robust this material could be and where its limitations lie in comparison to the pure PVDF. The output graphs are presented in Figure 39.

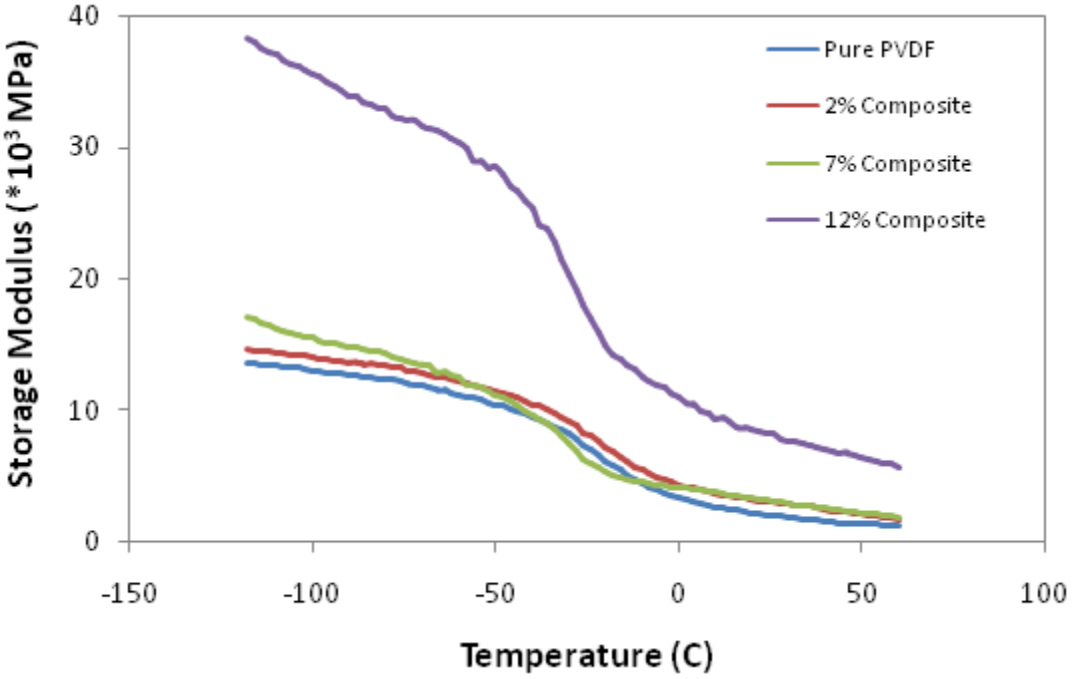

Figure 39: Effect of nanoparticles on storage modulus

Examining this image it is seen that with increasing concentrations of Fe_3O_4 there is a simultaneous rise in storage modulus of the material. Storage modulus is the material's ability to store energy. The increase is observed only in the composites which suggest the increase is due to the particles themselves. Miriyala et al. [51] showed that storage modulus increases in polymer composites are based in the networking between the particles. Being magnetic, the particles interact with each other even when embedded and these interactions grow with increasing amounts of particles. The increases in storage modulus for the 2% and 7% as show in Figure 39 are minor as compared to the sharp increase in the 12%. In the 2% and 7% case the PVDF properties are still dominating in terms of storage modulus and so the increase in modulus is minimal. In

the 12% case there is a greater level of particle-particle interaction and so a larger network formation, which now has greater influence on the modulus and causes the sharp increase [51]. The glass transition temperatures of the materials were observed and appeared to be shifting. The glass transition temperature represents the onset of long range molecular motion within a polymer. Table 9 shows the observed patterns found in the output, in relation to storage modulus and glass transition temperature.

Table 9: Effects on modulus and T_g

Sample	Storage Modulus (MPa) (@ -100°C)	T_g (°C)
Pure PVDF	13,056	-26
2%	13,580	-27
7%	15,569	-30
12%	35,368	-34

The glass transition temperature of this material is generally found around -30^{o}C [44]. This temperature can be located on the DMA outputs by finding the highest peak on the loss modulus graph [52]. Using analysis software the glass transition temperatures for each graph was obtained and tabled as shown in Table 9. Though slight, there is an observed shift in these transition temperatures, decreasing the T_g with increasing

amounts of magnetite nano-particles. The particles have a documented thermal conductivity value of 9.7 W/m K which is a lot greater than that of PVDF 0.17 W/m K[34]. Research done by Razzaq et al. concluded that, the thermal conductivity of polymer composites with fillers of greater thermal conductivity, increased with an increased concentration of filler [34]. Therefore with a higher thermal conductivity, the heat energy would be more efficiently conduced within the material and could explain the slight premature occurrences of the glass transition with increasing Fe_3O_4 concentration.

4.6. Melt and Crystallization

DSC provides a good analysis of the melt and re-crystallization behaviors of the material and works well as a compliment to the DMA results. Figure 40 is the DSC output results. It shows a comparison of output result of the pure PVDF vs. 12% PVDF/Fe_3O_4 sample. The solid line represents the pure PVDF while the dotted line represents the 12% sample.

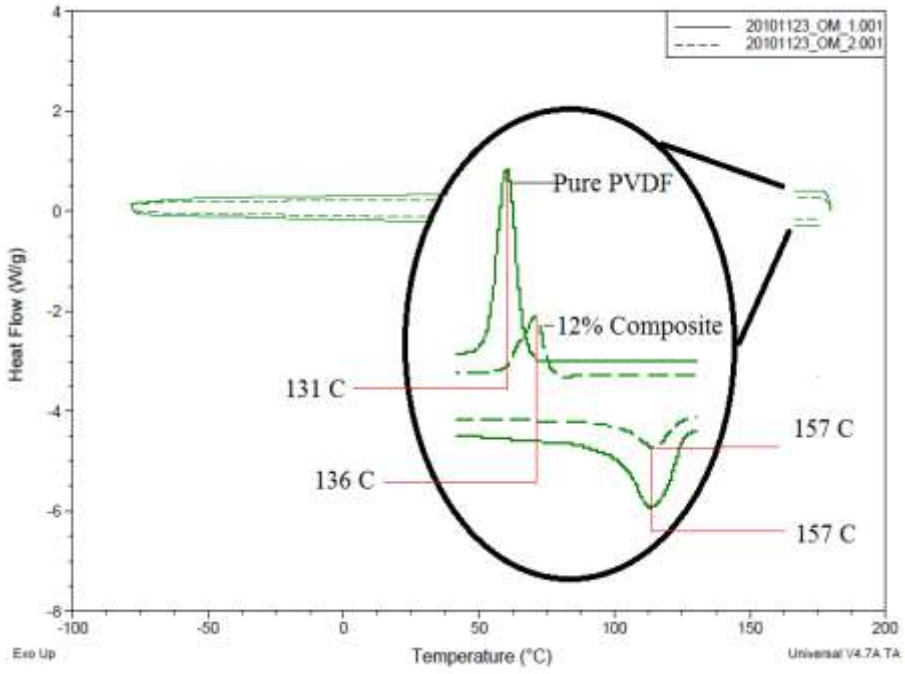

Figure 40: DSC comparison of pure PVDF vs. 12% PVDF/Fe_3O_4 sample

Examining this figure the two melting temperatures appear on the bottom right of the image. These values appear to coincide at the same temperature even though the heat of melting for the dotted 12% sample value is smaller. The thermal conductivity and diffusivity of a polymer matrix is increased when a filler of greater thermal conductivity is used to make a composite material [34]. Therefore analyzing the melting temperature peaks, the behavior can be attributed to the higher thermal parameters, the 12% sample requires less heat flow at the same temperature to achieve melt, while the pure PVDF requires more heat flow to melt.

The two peaks on the top half of the image represent the re-crystallization temperature. These are measure from a higher temperature to a lower temperature, as the sample is cooled from melt. The differences between the two samples are apparent. There is a shift to the right, or an increase in temperature at which re-crystallization happens. Also very noticeable is the drop in energy required to bring about re-crystallization. For re-crystallization to take place there must be a nucleation site from where to begin and then growth will be initiated [44, 47]. The polymer requires a certain amount of energy at a certain temperature for re-crystallization to occur. A reason for the shift is attributed the thermodynamics of the system and involves the role of the magnetite particles acting as nucleation sites to initiate crystallization. The increased conductivity of the composite is taken as responsible for the decrease in the required heat flow to achieve crystallization.

This chapter observed and studied the properties of this new class of composite materials. The next chapter discusses the energy conversion of the materials developed.

CHAPTER V

ENERGY ANALYSIS

This chapter discusses effects of Magnetite nano-particles on the piezoelectric behavior of PVDF. Estimation of the energy efficiency of the composite is provided at the later part of the chapter.

5.1. Piezoelectricity and the Effects of Fe_3O_4

As discussed in Chapter III, section 3.3.7, the energy performance was conducted using a linear stage. Results are shown in Figures 41-44, each figure showing a sample with different amounts of Fe_3O_4. Figure 41 shows the pure PVDF sample output of voltage measured using electrodes connected to the surface. The high point at -0.15V represents the 0V point. As time passes the sample is bent, and this bending produces an output which is observed as the peak. The maximum point is reached and the sample is straightened, returning to zero. The trend line of this peak represents the time dependent voltage v (t).This same process is repeated for the other composite samples in Figures 42-44. The outputs shown in Figures 43 and 44 are inverted so their zero point is found at around-0.3V and the max is around -0.15V.

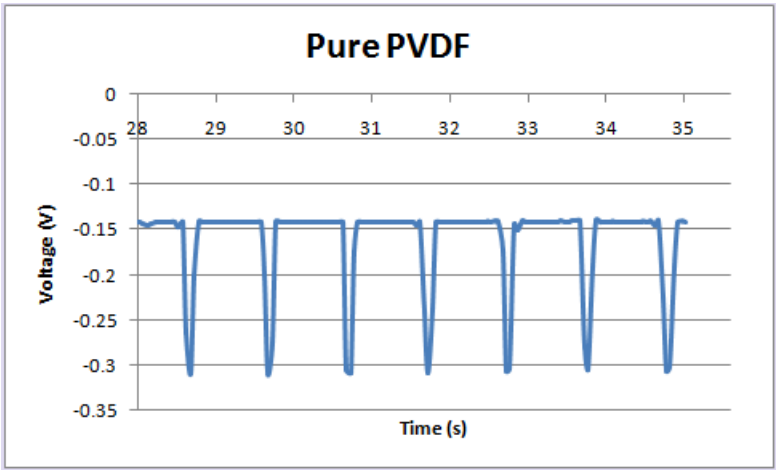

Figure 41: Pure PVDF voltage output

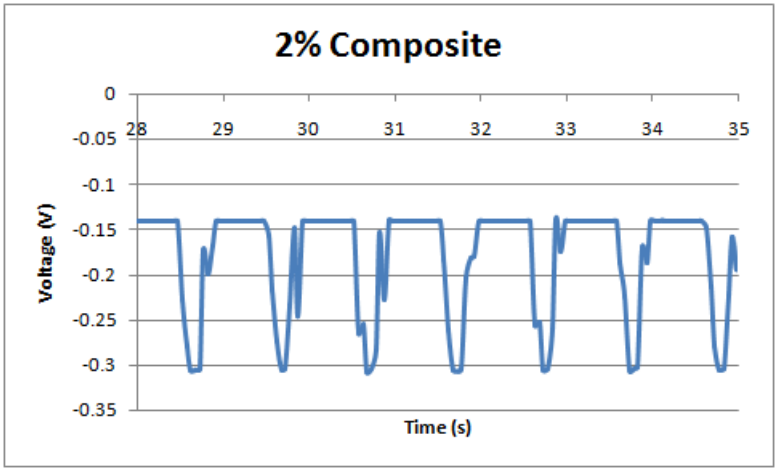

Figure 42: 2% composite voltage output

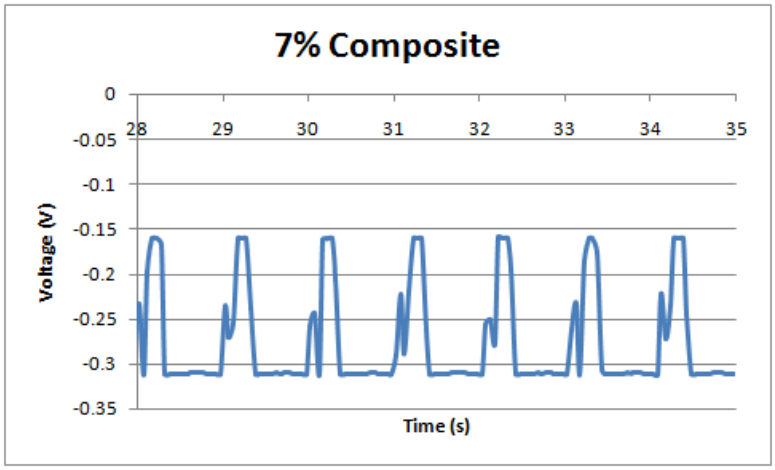

Figure 43: 7% composite voltage output

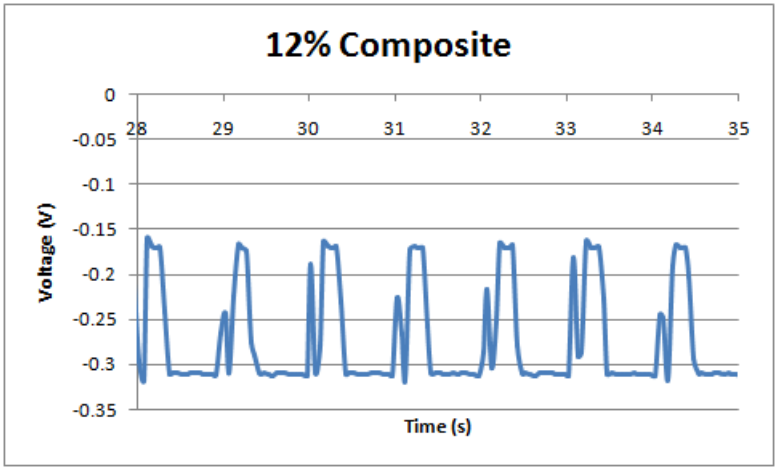

Figure 44: 12% composite voltage output

Observing Figures 41-44, it is seen that the shapes of the signal peaks differ. The PVDF, as a reference, has symmetric peaks throughout, whereas peaks found in the other materials are asymmetric. The separation of those asymmetric peaks is more pronounced with the increase of the Fe_3O_4 concentration.

As just mentioned, the asymmetry was observed in Figures 42-44, which are the samples containing the Fe_3O_4 particles. As discussed in Chapter III, section 3.3.7, all four samples were tested by bending. In the condition where no particles are added, the pure PVDF sample experienced no resistance and so the output plot comes out without blemish.

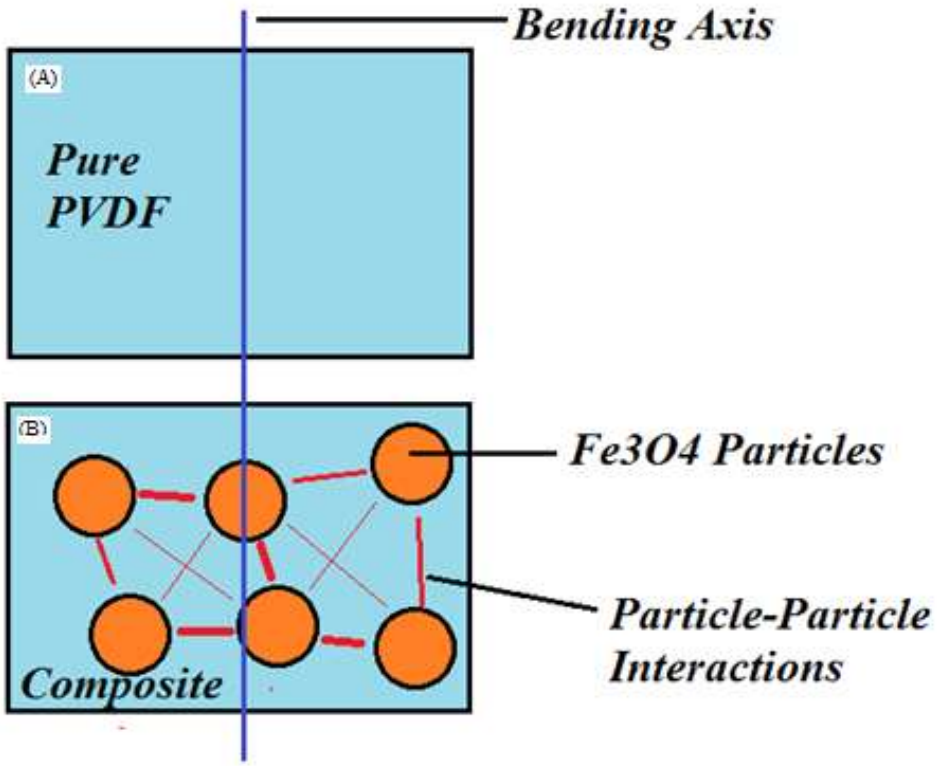

Figure 45: Example explaining effect of particles on material behavior

As shown in Figure 45, taking the blue line to represent the axis at which the samples are bent, it is observed from Figure 45A that the pure PVDF sample will experience no resistance. As was observed in the AFM results, in Chapter IV, the

Magnetite nano-particles are embedded in the matrix. This presence would already hinder bending with the particles playing the role of stress concentrators and not freely allowing the deformation. PVDF has been reported to show volume change as well as phase changes under stress conditions [53]. In this research the presence of the nanoparticles constrain the volume and phase change in the PVDF. The phase transformation from alpha phase into beta phase is hindered due to the presence of rigid Magnetite particles. The nanoparticles behave as hard spots resisting the volume expansion such that the final output voltage of PVDF would be reduced. Secondly there are the particle-particle interactions. These interactions bring with them an increased energy as a result of the forces that are being experienced between the particles. These forces and the presence of the particles are in opposition to deformation yet the force applied to bend the material is much greater and so the resistance is observed as the added smaller peaks which are overcome by the system.

Another observation made when comparing Figures 41-44 is that the time taken to reach the max point and return to zero is different and the trend lines representing the time dependent voltage, v (t). The equations of these lines forming the peaks can be obtained using Microsoft Excel as shown in Figure 46.

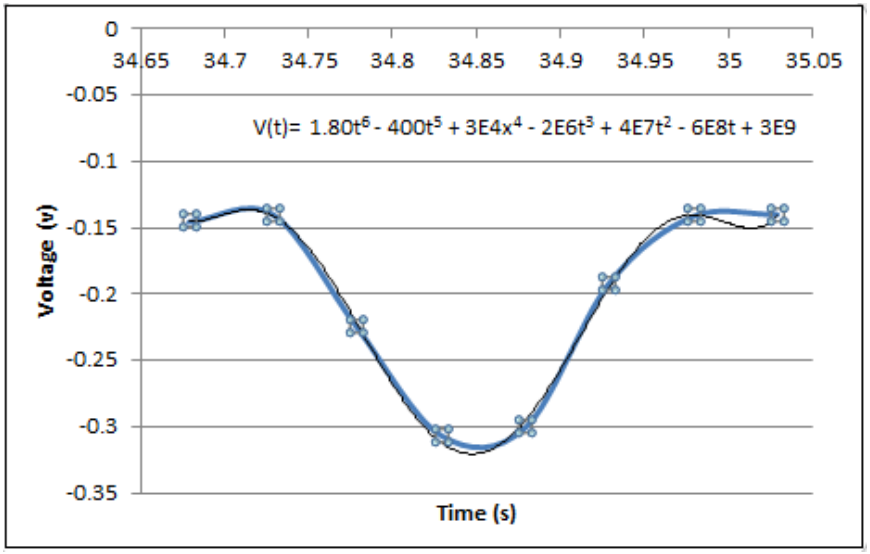

Figure 46: Example of the V (t) trend line

Using the trend lines and Equations (2)-(6) below, the energy properties of these materials can be calculated.

$$Q = 2 * d31 * c11 * \frac{W * T^3}{12 * L} * \frac{\pi^2 + 0.5\pi^2 * d + \in^3}{\pi\sqrt{d}} * (1 - d) \quad (2)$$

$$Trend\ line = V(t) \quad (3)$$

$$P = \int \frac{V(t) * Q}{t} dt \quad (4)$$

$$E = P * t \quad (5)$$

$$E = \int V(t) * Q dt \quad (6)$$

Here the symbol Q is the charge (C), P is the Power (W), E is the Energy (J), V is the Voltage (V), t is the Time (s), T is the thickness (m), W is the width (m), these and the rest of the symbols are summarized in Table 10.

Table 10: Equation parameters

SYMBOL	PARAMETER
Q	Charge (C)
P	Power (W)
E	Energy (J)
V	Voltage (V)
t	Time (s)
T	Thickness (m)
W	Width (m)
d31	Strain Constant
c11	Elastic Constant
L	Length (m)
d	Deflection(m)
ε	Permittivity (F/m)

Equation (2) is the charge produced by a piezoelectric material; it is dependent on piezoelectric constants and sample dimensions. The starting point is finding the output time dependent voltage in Equation(3) for the peak being analyzed, as shown in Figure 46. This equation will be representative of the time dependent voltage as shown in Equation (3).

The energy is formulated in Equation (6), it is achieved by substituting the power Equation (4) into the energy Equation (5).

It is observed in Figures 41-44 that the peaks occur at specific time intervals, therefore these are the time intervals over which the time dependent voltage will be integrated. Using the time dependent voltage and the charge calculated using Equation (2), the energy produced over the interval can be obtained using Equation (6).

The observed effects in Figures 41-44 have been related to the presence of the particles, so they are also responsible for increased time taken to reach max and return to zero. In addition it appears that the increase in time is related to the increase in particles, for example Figure 44 taking a longer time than Figure 42. In the discussions regarding the added peaks it was observed that particle-particle interactions had to be overcome to reach max and return to zero. With more particles in the same square area there exists more interaction and so more resistance to overcome to complete cycle. This would explain the extended time with increased amount of particles. The calculated energy results are show in Figure 47.

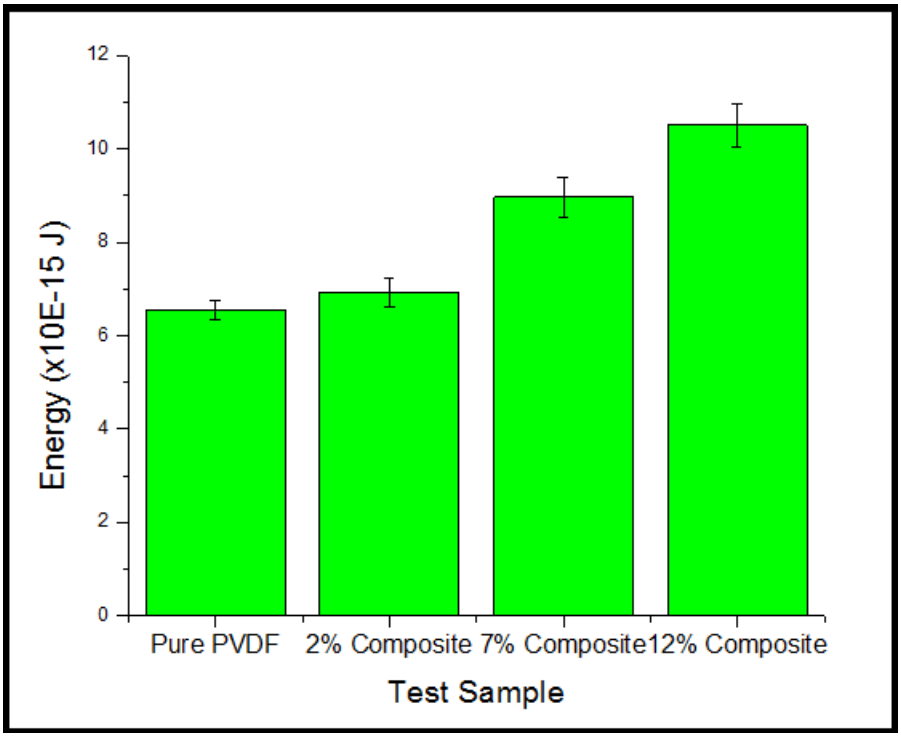

Figure 47: Energy increase due to particles

It is observed that with increasing amounts of Fe_3O_4 particles, there is an increase in the energy property of the material. This result is in agreement with the DMA results, which showed that increasing the amount of Fe_3O_4 particles caused an increase in the storage modulus. Storage modulus is representative of a material's ability to store energy. It was discussed that the particle-particle interactions represented energy due to the forces between the particles, and so with an increase in the amount of particles there would also be an increase in these forces. Calculations were done to observe how much of an improvement was achieved in comparison to the pure PVDF, the results are tabulated in Table 11.

Table 11: Energy increase due to particles

SAMPLE	% ENERGY INCREASE
2% Composite	5%
7% Composite	26%
12% Composite	37%

These results in Table 11 re-iterate that there is an increase in the energy with an increase in the amount of Fe_3O_4 particles. When observed closely it is also apparent that the increase in energy from the 2% to 7% sample is greater than the jump from the 7% to the 12% sample. This could be indicating that the increase in energy due to the particles could be topping out and reaching a saturation point. This may be attributed to the small size of sample, yet since the particle dispersion was performed by "percent by weight", it would be expected that similar result would be viewed with bigger samples as well.

All the tests to this point were conducted in ambient (air). Since the Fe_3O_4 particles are magnetic and have the magnetostriction property, the same tests were conducted within a magnetic field. The magnetic field was provided by an electromagnet and its intensity was measured at B = 0.0042 Teslas using a Hall Effectmeter. The value 0.0042 Teslas is equivalent to magnetization of a fridge magnet. The tests were run and the results are presented in comparison to the ambient (air) results as shown in Figures 48-50.

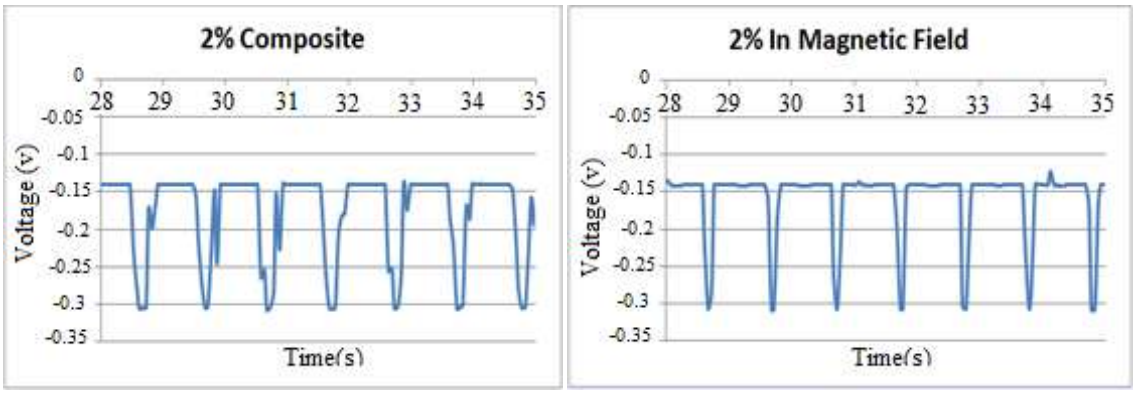

Figure 48 : Visual of magnetic field effect on voltage outputs in comparison to the result without the magnetic field (2%)

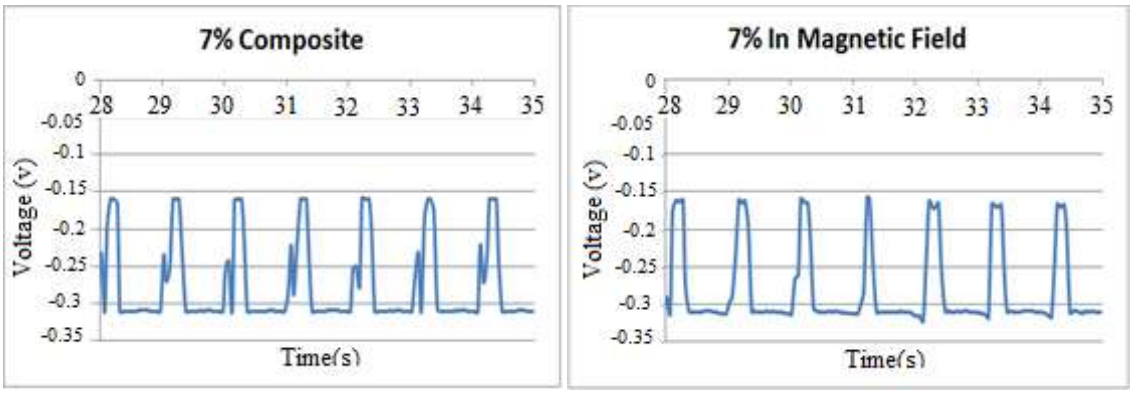

Figure 49: Visual of magnetic field effect on voltage outputs in comparison to the result without the magnetic field (7%)

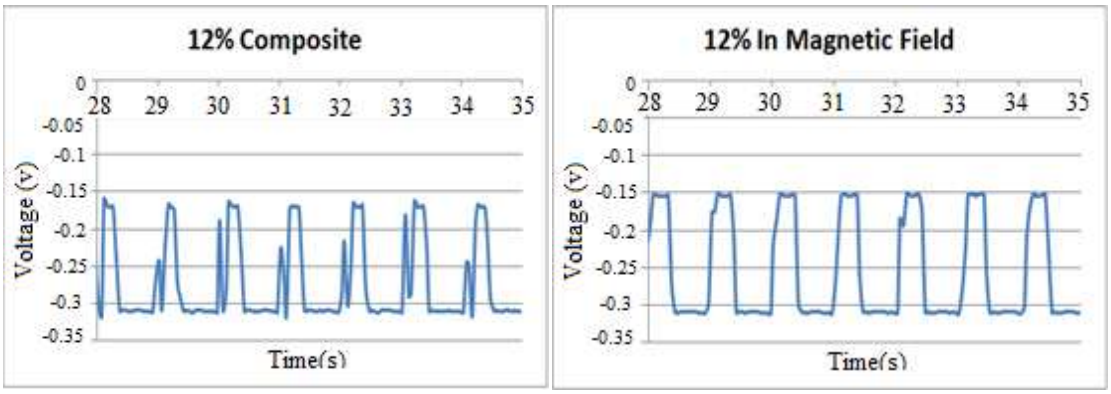

Figure 50: Visual of magnetic field effect on voltage outputs in comparison to the result without the magnetic field

The pure PVDF did not contain any particles and as expected when tested, no change was observed. The effect of the presence of the magnetic field on the composite samples is visually observed, as the previously seen added peaks are no longer present. An important observation is that the particles, though embedded in the PVDF matrix as seen in the AFM results in chapter IV, are still responsive to the externally applied magnetic field. The importance of this observation lies in the fact that this may provide a new dimension in the activation of piezoelectric based devices. The majority of piezoelectric devices have relied on vibration, motion or force to activate them. In this case the magnetic field's ability to trigger the particles embedded in the PVDF matrix shows the potential to harness more than one type of energy in this single material.

The effect of the magnetic field, as seen in Figures 48-50, was observed as changes in the trend line equations and the time taken to complete a peak. In these figures, the difference between each sample was affected by the applied magnetic field without changing the trend. A common point for all samples containing particles was

that the output potential was reduced when placed in a magnetic field. The possible reasons are illustrated in Figure 51; it presents possibilities in terms of the effects of the nanoparticles.

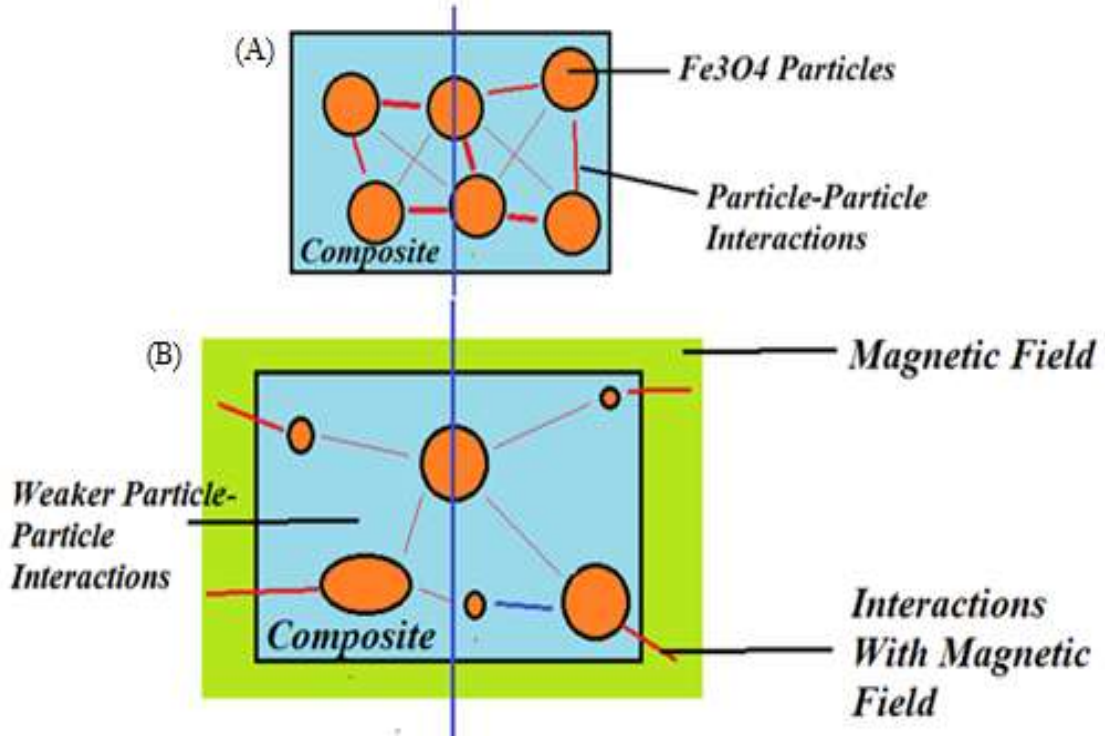

Figure 51: Example explaining effect of magnetic field on voltage

Figure 51 above is a comparison of behavior between the composite in ambient (air, 51A) and the composite within the magnetic field (51B).

When placed in a magnetic field, there is an increase in interactions between particles. Such interactions would further constrain the change of PVDF where phase transformation is needed for producing needed output voltage. Secondly the Fe_3O_4 possesses a property called magnetostriction. The magnetostriction property of Fe_3O_4 causes the particles to change their dimensions or shape when placed within a magnetic field, as shown in Figure 51B[54]. The particles can either expand or contract depending on the orientation of magnetic field. Studies have shown that these particles do not expand or contract along all their axes, some experience expansion while others contract. The effects of the magnetostriction as well as that of the magnetic field and particle interactions are accepted to be responsible for the behavior of the material. With the alterations observed in the trend lines and peak times for Figures 48-50, another set of energy calculations were performed to observe the effect of the magnetic field on the energy property of the material. Figure 52 presents the results of these calculations in comparison to the results obtained in the ambient air calculations.

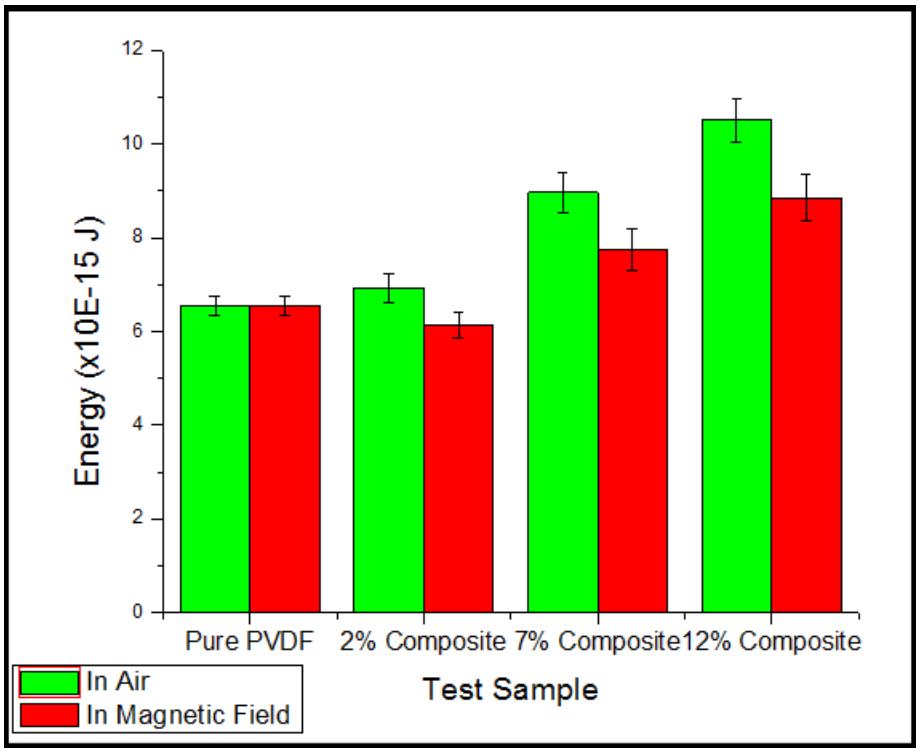

Figure 52: Effects of magnetic field on energy property

It is observed that the presence of the magnetic field causes a decrease in the energy of the materials. As viewed with the voltage graphs in Figures 48-50, the magnetic field was responsible for the lessening of the added peaks. Figures 41-44 showed that there was an increase in energy as a result of the interactions of the nanoparticles. The applied magnetic field however reduced the overall increase in output energy.

Overall, the 7% and 12% samples show the highest voltage production compared to the pure PVDF. With PVDF being a widely used material in both research and application, an improvement in its capabilities could allow for much improvement in

existing applications and provide possibilities for new ones. In addition to the superior output, the observed interaction with the magnetic field and its effect on the samples has introduced another dimension of activation for these types of materials. The majority has been related to vibrations and physical motion or force, incorporating a magnetic possibility with increased output could open the door to numerous possibilities in terms of inventive applications and research.

CHAPTER VI

CONCLUSIONS

This research set out to develop a material possessing enhanced properties by combining materials with functional properties. A composite was developed made of Polyvinylidenefluoride and Magnetite nanoparticles. This composite showed an enhancement in its energy outputs in comparison to the pure PVDF samples as shown in Figure 53.

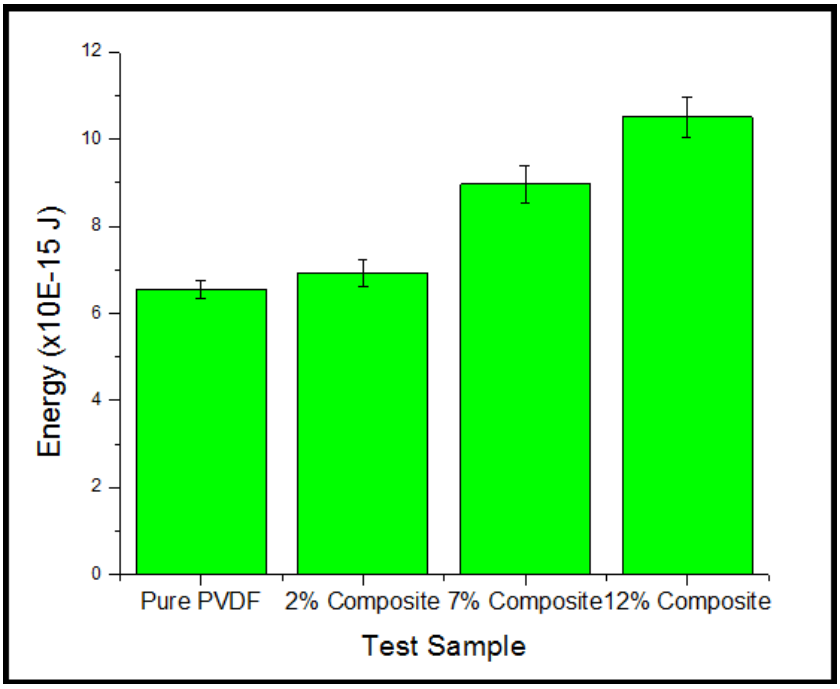

Figure 53: Particles cause energy increases

Table 12: Observed improvements in energy

SAMPLE	% ENERGY INCREASE
2% Composite	5%
7% Composite	26%
12% Composite	37%

The magnitude of increase is shown in Table 12. These increases are in comparison to the pure PVDF sample output.

This research also showed that the embedded nanoparticles interacted with an exteriorly applied magnetic field. This was observed by running the same tests within a magnetic field. The results are as shown in Figure 54.

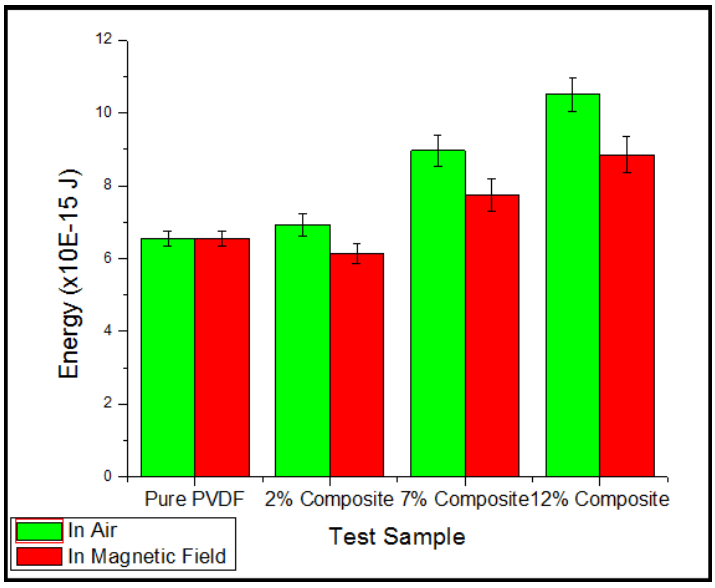

Figure 54: Magnetic field causes a decrease in output energy

Decreases are observed in the sample outputs when placed within a magnetic field, which indicated an interaction with the magnetic field. This observation introduces a new dimension of possible activation processes for piezoelectric devices which have been largely based on physical forms of activation. PVDF which is widely used in research and applications for its superior output capabilities has been enhanced in this research and shown to exhibit higher output capabilities. Above the induced enhancement of the material, the observation of the embedded particle interaction with the magnetic field introduces a new dimension of possible activation processes for piezoelectric devices which have been largely based on physical forms of activation.

REFERENCES

[1] D. Jourdan. Still growing business but unit prices are decreasing and infrastructure changes are needed 2007. Micronews. 43. [Online]. Available: http://www.yole.fr/pagesAn/micronews/Old_Micronews/MN59.pdf

[2] R. Whitney. Nellis activates Nations largest PV Array 2007. [Online]. Available: http://www.shinesolar.net/index.php/News/Disp/nid/69

[3] W. Choi. Dye sensitive solar cell 2009. [Online]. Available: http://web.eng.fiu.edu/choiwweb/dssc

[4] D. Hopwood. Belgium inaugurates wind farm with largest wind turbines 2009. [Online]. Available: http://www.renewableenergyfocus.com/view/5588/belgium-inaugurates-wind-farm-with-largest-wind-turbines

[5] Seiko. Kinetic. A powerhouse of technological innovation 2007. [Online]. Available: http://www.seikowatches.com/technology/kinetic/index.html

[6] Nokia. Applications of Nanoscale Zinc Oxide. Nokia Technology Insights series 2008. [Online]. Available: http://research.nokia.com/files/NTI_Nanoscience_-_Dec_2008.pdf

[7] Yichang. Wide shot of the Three Gorges dam 2007. [Online]. Available: http://www.iihr.uiowa.edu/education/international/china07/images/wuhan21_0002_large.jpg

[8] Y. Liang, S. Xiao, D. Feng, and L. Yu, "Control in energy levels of conjugated polymers for photovoltaic application," The Journal of Physical Chemistry C, vol. 112, pp. 7866-7871, 2008.

[9] S. Roundy, V. Sundararajan, J. Baker, E. Carleton, E. Reilly, et al., "Energy scavenging in support of ambient intelligence - Techniques, challenges, and future directions," in AmIware: Hardware Technology Drivers of Ambient Intelligence. vol. 5, S. Mukherjee, et al., Eds., Netherlands: Springer, 2006, pp. 265-284.

[10] C. B. Williams, C. Shearwood, M. A. Harradine, P. H. Mellor, T. S. Birch, et al., "Development of an electromagnetic micro-generator," IEE Proceedings Circuits, Devices and Systems,, vol. 148, pp. 337-342, 2001.

[11] C. R. Saha, T. O'Donnell, N. Wang, and R. McCloskey, "Electromagnetic generator for harvesting energy from human motion," Sensors and Actuators A-Physical, vol. 147, pp. 248-253, 2008.

[12] D. Guyomar, G. Sebald, S. Pruvost, M. Lallart, A. Khodayari, et al., "Energy harvesting from ambient vibrations and heat," Journal of Intelligent Material Systems and Structures, vol. 20, pp. 609-624, 2009.

[13] C. B. Williams and R. B. Yates, "Analysis of a micro-electric generator for microsystems," Sensors and Actuators A: Physical, vol. 52, pp. 8-11, 1995.

[14] T. Starner, "Human-powered wearable computing," IBM Systems Journal, vol. 35, pp. 618-629, 1996.

[15] J. Kymissis, C. Kendall, J. Paradiso, and N. Gershenfeld, Parasitic Power Harvesting in Shoes: IEEE Press, 1998.

[16] J. S. Harrison and Z. Ounaies, Polymers, Piezoelectric. Hampton, VA: John Wiley & Sons, Inc., 2002.

[17] W. G. Cady, "Piezoelectricity and ultrasonics," Sound, vol. 2, pp. 46-53, 1963.

[18] T. Ikeda, Fundamentals of Piezoelectricity. New York: Oxford University Press, 1990.

[19] G. M. Sessler, "Piezoelectricity in polyvinylidene fluoride," Journal of the Acoustical Society of America, vol. 70, pp. 1596-1608, 1981.

[20] G. Gautschi, Piezoelectric Sensorics. Berlin: Springer, 2002.

[21] J. Singh, Smart Electronic Materials: Fundamentals and Applications. Cambridge: Cambridge University Press, 2005.

[22] D. Klimm, "Piezoelectricity," Crystal Research and Technology, vol. 23, pp. 1538-1538, 1988.

[23] A. Arnau, Piezoelectric Transducers and Applications. New York: Springer, 2004.

[24] G. Pauliat, P. Mathey, and G. Roosen, "Influence of piezoelectricity on the photorefractive effect," Journal of the Optical Society of America B-Optical Physics, vol. 8, pp. 1942-1946, Sep 1991.

[25] H. Kawai, "Piezoelectricity of poly(vinylidene fluoride)," Japanese Journal of Applied Physics, vol. 8, pp. 975-977, 1969.

[26] K. Nakamura and Y. Wada, "Piezoelectricity, pyroelectricity, and electrostriction constant of poly(vinylidene fluoride)," Journal of Polymer Science Part A-2-Polymer Physics, vol. 9, pp. 161-164, 1971.

[27] J. G. Bergman, J. H. McFee, and G. R. Crane, "Pyroelectricity and optical second harmonic generation in polyvinylidene fluoride films," Applied Physics Letters, vol. 18, pp. 203-205, 1971.

[28] A. M. Vinogradov, S. C. Schumacher, and E. M. Rassi, "Dynamic response of the piezoelectric polymer PVDF," International Journal of Applied Electromagnetics and Mechanics, vol. 22, pp. 39-51, 2005.

[29] T. K. James Jacobs, Engineering Materials Technology. Upper Saddle River, NJ: Prentice Hall, 2004.

[30] A. J. Lovinger, "Ferroelectric polymers," Science, vol. 220, pp. 1115-1121, 1983.

[31] R. Hasegawa, Takahash.Y, H. Tadokoro, and Y. Chatani, "Crystal-structures of 3 crystalline forms of poly(vinylidene fluoride)," Polymer Journal, vol. 3, pp. 600-602, 1972.

[32] M. A. Bachmann, W. L. Gordon, S. Weinhold, and J. B. Lando, "The crystal-structure of phases-IV of poly(vinylidene fluoride)," Ferroelectrics, vol. 30, pp. 95-95, 1980.

[33] G. Eberle, H. Schmidt, and W. Eisenmenger, "Piezoelectric polymer electrets," IEEE Transactions on Dielectrics and Electrical Insulation, vol. 3, pp. 624-646, Oct 1996.

[34] M. Y. Razzaq, M. Anhalt, L. Frormann, and B. Weidenfeller, "Thermal, electrical and magnetic studies of magnetite filled polyurethane shape memory polymers," Materials Science and Engineering A-Structural Materials Properties Microstructure and Processing, vol. 444, pp. 227-235, Jan 2007.

[35] W. Moller, S. Takenaka, M. Rust, W. Stahlhofen, and J. Heyder, "Probing mechanical properties of living cells by magnetopneumography," Journal of Aerosol Medicine-Deposition Clearance and Effects in the Lung, vol. 10, pp. 173-186, 1997.

[36] G. Bate, "Particulate recording materials," Proceedings of the IEEE, vol. 74, pp. 1513-1525, 1986.

[37] S. Wei, Y. Zhu, Y. Zhang, and J. Xu, "Preparation and characterization of hyperbranched aromatic polyamides/Fe3O4 magnetic nanocomposite," Reactive and Functional Polymers, vol. 66, pp. 1272-1277, 2006.

[38] G. Qiu, Q. Wang, and M. Nie, "Polyaniline/Fe3O4 magnetic nanocomposite prepared by ultrasonic irradiation," Journal of Applied Polymer Science, vol. 102, pp. 2107-2111, 2006.

[39] J. Y. L. Bong Shik Kim, Roger S Porter, "The crystalline phase transformation of poly(vinylidene fluoride)/poly(vinyl fluoride) blend films," Polymer Engineering and Science., vol. 38, p. 7, 1998.

[40] J. A. Giacometti and O. N. Oliveira, Jr., "Corona charging of polymers," IEEE Transactions on Electrical Insulation, vol. 27, pp. 924-943, 1992.

[41] S. N. Magonov and M. G. Heaton, "Scanning probe microscopy part 3: Studies of polymer surfaces with atomic force microscopy," American Laboratory, vol. 28, pp. 59-63, 1996.

[42] J. Shirakashi, K. Matsumoto, N. Miura, and M. Konagai, "Single-electron transistors (SETs) with Nb/Nb oxide system fabricated by atomic force microscope (AFM) nano-oxidation process," Japanese Journal of Applied Physics, Part 2 (Letters), vol. 36, pp. 1257-1260, 1997.

[43] D. J. Muller, D. Fotiadis, S. Scheuring, S. A. Muller, and A. Engel, "Electrostatically balanced subnanometer imaging of biological specimens by atomic force microscope," Biophysical Journal, vol. 76, pp. 1101-11, 1999.

[44] W. Callister, Materials Science and Engineering: An Introduction: John Wiley & Sons, 2006.

[45] D. M. Esterly and B. J. Love, "Phase transformation to -poly(vinylidene fluoride) by milling," Journal of Polymer Science, Part B: Polymer Physics, vol. 42, pp. 91-97, 2004.

[46] G. Laroche, C. P. Lafrance, R. E. Prud'homme, and R. Guidoin, "Identification and quantification of the crystalline structures of poly(vinylidene fluoride) sutures by wide-angle X-ray scattering and differential scanning calorimetry," Journal of Biomedical Materials Research, vol. 39, pp. 184-189, 1998.

[47] P. Hiemenz, Polymer chemistry: CRC Press, 2007.

[48] A. Jain, J. Kumar S, D. R. Mahapatra, and H. H. Kumar, "Detailed studies on the formation of piezoelectric -phase of PVDF at different hot-stretching conditions," in Sensors and Smart Structures Technologies for Civil, Mechanical, and Aerospace Systems 2010, March 8, 2010 - March 11, 2010, San Diego, CA, United states, 2010, pp. The Society of Photo-Optical Instrumentation Engineers (SPIE); American Society of Mechanical Engineers; KAIST.

[49] A. Salimi and A. A. Yousefi, "Conformational changes and phase transformation mechanisms in PVDF solution-cast films," Journal of Polymer Science, Part B (Polymer Physics), vol. 42, pp. 3487-95, 2004.

[50] S. G. Satapathy, P. K.; Pawar, Santosh; Varma, K. B. R., "Crystallization of Beta-phase Poly (vinylidene fluoride) films using dimethyl sulfoxide (DMSO) solvent and at suitable annealing condition," 2008.

[51] S. M. Miriyala, Y. S. Kim, L. Liu, and J. C. Grunlan, "Segregated networks of carbon black in Poly(vinyl acetate) latex: Influence of clay on the electrical and mechanical behavior," Macromolecular Chemistry and Physics, vol. 209, pp. 2399-2409, 2008.

[52] K. Menard, Dynamic Mechanical Analysis: A practical introduction, Second Edition: CRC Press, 2008.

[53] H. Lee, R. Cooper, K. Wang, and H. Liang, "Nano-scale characterization of a Piezoelectric polymer (Polyvinylidene Difluoride, PVDF)," Sensors, vol. 8, pp. 7359-7368, 2008.

[54] C. W. Heaps, "The magnetostriction of a Magnetite crystal," Physical Review, vol. 24, p. 60, 1924.

VITA

Oliver Kasongo Mulamba received his Bachelor of Science degree in mechanical engineering from West Texas A&M University in 2009. He entered the mechanical engineering master's program at Texas A&M University in September 2009, and received his Master of Science degree in May 2011. Though having a broad range of interests, his research area focused on the synthesis and characterization of piezoelectric composites. Mr. Mulamba will be furthering his education and pursuing his Ph.D in mechanical engineering. He may be reached at Texas A&M University, Department of Mechanical Engineering, 3123 TAMU, College Station TX 77843-3123. His email address is okmulamba@yahoo.com.